

Multiterminal ballistic Josephson junctions coupled to normal leads

Régis Mélin¹

¹Univ. Grenoble-Alpes, CNRS, Grenoble INP, Institut NEEL, 38000 Grenoble, France

Nonequilibrium multiterminal superconducting devices have focused considerable interest recently in connection with Floquet theory and/or nontrivial topology. In the paper, we address physically-motivated approximations for the time-periodic Floquet dynamics in a finite geometry. The problem is nontrivial in time and in space. We assume that nonproximitized regions are formed in between the superconducting leads evaporated on top of a two-dimensional metal. We demonstrate relevance of phenomenological superconducting double quantum dots to the two-Cooper pair resonance. The following features emerge from the calculations: (i) Enhancement of the quartet phase-sensitive critical current is produced by small coupling to the normal lead attached to the device; (ii) Fraction of the current is transmitted through the normal parts of the circuit; (iii) Voltage-tunable cross-overs appear between “inversion” and “absence of inversion”, where “inversion” refers to the counterintuitive larger critical current at half flux-quantum than in zero field. We present numerical calculations for single-channel contacts, producing log-normal variations of the quartet critical current with bias voltage. Qualitative compatibility with the recent Harvard group experiment is pointed out. Perspectives involve the interplay between the “non-selfaveraging-like” Floquet resonance peaks in the voltage dependence of the quartet critical current, and the averaging effects of extended interfaces or bias voltage fluctuations.

I. INTRODUCTION

BCS superconductors [1] are characterized by macroscopic phase variable φ and energy gap Δ between the ground state and the first quasiparticles. The Cooper pairs are nonentangled as long as they stay in the bulk of a BCS condensate. In superconductor-normal metal (SN) structures, the direct BCS attractive interaction is solely operational in the superconductor S , but the Cooper pairs from S can be transmitted as Andreev pairs into the normal part N of the junction, keeping their two-electron superconducting coherence at long distance from the interface. Those entangled Andreev pairs have the opportunity to split if two independent voltages are applied in three-terminal F_aSF_b ferromagnet-superconductor-ferromagnet or N_aSN_b normal metal-superconductor-normal metal Cooper pair beam splitters [2–29]. “Nonlocal Andreev reflection” or, said differently, “crossed Andreev reflection” (CAR) appears if the separation between the N_aS and SN_b interfaces is comparable to the zero-energy superconducting coherence length. Spin-up electron from lead N_b can be Andreev reflected as spin-down hole into N_a , leaving a Cooper pair in the “central” S . As a result of those nonlocally split Cooper pairs, the current I_a through N_a is sensitive to the bias voltage V_b on N_b [2–29]. In addition, the positive current-current cross-correlations of Cooper pair splitting [4, 30–41] were experimentally revealed [23, 24].

Regarding those normal metal-superconductor-normal metal Cooper pair beam splitters [16–29], the double quantum dot experiments [21, 22, 24] provide evidence for non-local two-particle Andreev resonance in N_a -dot- S_c -dot- N_b devices, on the condition of the opposite energy levels $\varepsilon_a = -\varepsilon_b$ on both quantum dots. In the following, we demonstrate how “nonlocal two-particle Andreev resonance” in N_a -dot- S_c -dot- N_b Cooper pair beam splitters can be generalized to “nonlocal two-Cooper pair resonance” in all-superconducting three-terminal Josephson junctions.

Those two-Cooper pair resonances build on nonlocal two-Cooper pair states, the so-called quartets [42–56] that appear in (S_a, S_c, S_b) three-terminal Josephson junctions, where S_a

and S_b are voltage-biased at V_a and V_b , the superconducting lead S_c being grounded at $V_c = 0$. Andreev scattering yields quartet phase-sensitive DC-current response if the condition $V_a = -V_b \equiv V$ is fulfilled. On this quartet line $V_a = -V_b$, the elementary transport process transfers two Cooper pairs from S_a and S_b into the grounded S_c , while exchanging partners [42–56]. By the time-energy uncertainty relation, this phase-sensitive quartet current is DC, since, on the quartet line, the energy $E_i = 2e(V_a + V_b)$ of two Cooper pairs from S_a and S_b in the initial state is equal to the final state energy $E_f = 4eV_c$ of the two Cooper pairs transmitted into S_c .

Several experiments were recently performed on multiterminal Josephson junctions [57–66]. Some of those explored the possibility of nontrivial topology [56, 58, 67–83]. On the other hand, three groups reported compatibility with the quartets [42–56]: the Grenoble group experiment with metallic structures [57], the Weizmann Institute group experiment with semiconducting nanowires [59] and the more recent Harvard group experiment on ballistic graphene-based four-terminal Josephson junctions [61]. This third experiment [61] is summarized in figures 1a and 1b. The latter shows the typical experimental variations for the quartet critical current as a function of the bias voltage V and the magnetic flux Φ through the loop. The experiment features the counterintuitive voltage- V -tunable inversion, i.e. the possibility of stronger quartet critical current at half-flux quantum $\Phi = \pi$ than in zero field $\Phi = 0$, see figure 1b. The present paper is motivated by exploring interpretation of this experiment, in the continuation of our previous papers I and II [51, 52].

Zero-dimensional (0D) quantum dots were used in Ref. 84 to model two-terminal graphene-superconductor hybrids, in connection with experimental evidence for the Floquet replica of the Andreev spectrum under microwave radiation. The goal of the present paper is to similarly describe four-terminal graphene-based Josephson junctions with effective models based on quantum dots. We argue that multilevel quantum dots coupled to four superconducting and a normal lead are “minimal models” of four-terminal Josephson junctions that are intermediate between the short- and long-junction limits.

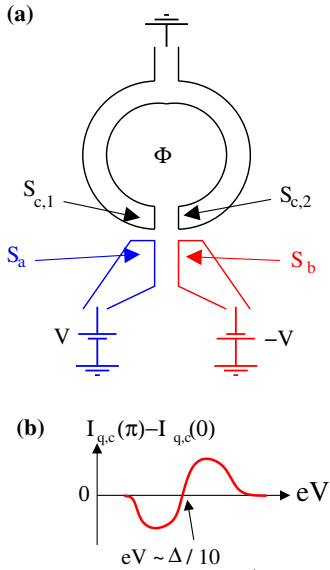


FIG. 1. *Schematic four-terminal experiment:* Panel a represents top-view of the experimental device, with the superconducting leads S_a and S_b biased at $V_{a,b} = \pm V$. The loop terminated by $S_{c,1}$ and $S_{c,2}$ is connected to ground by the contact on top of it, and it is pierced by the magnetic field flux Φ . The four superconducting leads are evaporated on a graphene layer gated far from the Dirac point, and forming a two-dimensional (2D) metal. Panel b summarizes the experimental result [61] that inspires the present theoretical paper, i.e. the quartet critical current current $I_{q,c}(\pi)$ at flux $\Phi = \pi$ can be larger or smaller than $I_{q,c}(0)$ at flux $\Phi = 0$, in a way that is sensitive to voltage typically being in the range $eV \approx \Delta/10$ where Δ is the superconducting gap.

In addition, we further simplify the description in terms of double 0D quantum dots. Four or more Andreev bound states (ABS) are within the gap in the equilibrium limit, instead of two ABS for a single 0D quantum dot.

Importantly, nonproximitized regions can appear in the two-dimensional (2D) metal, typically in the “cross-like region” formed in between the contacts with the superconductors, see figure 1a. Then, the quantum transport process can have initial or final states in those normal regions of the circuit. Current lines can be converted by Andreev reflection as supercurrent flowing in the grounded superconducting loop. Namely, current conservation for symmetric coupling to the superconducting leads implies that the 2D metal chemical potential is at the same zero energy as that of the superconducting loop. Thus, the normal carriers transmitted through the 2D metal can be transferred into the grounded superconducting loop without taking or giving energy.

Now, we explain the connection between the present work and our previous papers. Compared to our previous Ref. 47, we implement a double 0D quantum dot, instead of the single quantum dot Dynes parameter [85–88] model of Ref. 47. We also include four superconducting leads, instead of three in our previous Ref. 47. Our previous paper I [51] presented an expansion of the quartet critical current in perturbation in the tunneling amplitudes between a 2D metal and four superconducting leads. The present paper addresses resonances that

appear beyond the weak coupling limit. Our previous paper II [52] treated single quantum dot with relaxation solely originating from the continua of BCS quasiparticles. Relaxation then produces nonvanishingly small line-width broadening δ_0 for the Floquet resonances, which behaves like $\log \delta_0 \sim -\Delta/eV$ at low bias voltage energy eV compared to the superconducting gap Δ [47, 48, 52, 78]. In the four-terminal device of paper II [52], Landau-Zener quantum tunneling reduces the quartet current by coherent superpositions in the dynamics of the two opposite current-carrying ABS, at voltage values that are close to avoided crossings in the Floquet spectra. This mechanism is analogous to the reduction of the DC-Josephson current in microwave-irradiated weak links [89]. Conversely, in the present work, the interplay between the time-periodic dynamics and finite line-width broadening due to the attached normal lead restores the expected sharp resonance peaks in the voltage-dependence of the quartet current. For instance, a resonantly driven harmonic oscillator has amplitude inverse proportional to the damping rate. In addition, we note that the zero-frequency noise of a single superconducting weak link at finite temperature is inverse proportional to the rate set by the Dynes parameter [85–88] in some parameter window, see Ref. 90. The same scaling holds in this reference for the noise at frequency $2\omega_S$, where ω_S is the ABS energy. The quartets in four-terminal devices [51, 52, 61] offer several parameters to probe this physics, such as the quartet phase variable and the “knobs” of the bias voltage and magnetic flux.

The paper is organized as follows. The Hamiltonians are presented in section II. The mechanism for the two-Cooper pair resonance is discussed in section III. The mechanism for the inversion is presented in section IV. Section V shows numerical results. Concluding remarks are presented in the final section VI.

II. HAMILTONIANS

In this section, we provide the Hamiltonians on which the paper is based. Subsection II A presents the general Hamiltonians of the superconductors, quantum dots and normal leads. Subsection II B presents the Hamiltonians of the specific devices considered in the paper.

A. General Hamiltonians

Now, we present the general Hamiltonians. Subsection II A 1 presents the BCS Hamiltonian of the superconducting leads. Subsections II A 2 and II A 3 introduce the Hamiltonians of the quantum dots and normal leads respectively.

1. Superconductors

Now, we present the Hamiltonian of the superconducting leads.

The Hamiltonian of a BCS superconductor is the following:

$$\mathcal{H}_{BCS} = -W \sum_{\langle i,j \rangle} \sum_{\sigma_z=\uparrow,\downarrow} \left(c_{i,\sigma_z}^+ c_{j,\sigma_z} + c_{j,\sigma_z}^+ c_{i,\sigma_z} \right) - \Delta \sum_i \left(\exp(i\varphi_i) c_{i,\uparrow}^+ c_{i,\downarrow} + \exp(-i\varphi_i) c_{i,\downarrow} c_{i,\uparrow} \right), \quad (1)$$

where $\sum_{\langle i,j \rangle}$ denotes summation over pairs of neighboring tight-binding sites labeled by i and j , and σ_z is the component of the spin along quantization axis. The bulk hopping amplitude is denoted by W and the superconducting gap Δ is taken identical in all superconducting leads S_a , S_b , $S_{c,1}$ and $S_{c,2}$. The variable φ_i denotes the superconducting phase variable at the tight-binding site labeled by i . In the following, the current is weak and φ_i is approximated as being uniform in space, with the values φ_a , φ_b , $\varphi_{c,1}$, and $\varphi_{c,2}$ in S_a , S_b , $S_{c,1}$ and $S_{c,2}$ respectively.

We assume short distance between the contact points c_1 and c_2 (at the interfaces between $S_{c,1}$ or $S_{c,2}$ and the quantum dot), and we use the approximation of the gauge

$$\varphi_{c,1} = \varphi_c \quad (2)$$

$$\varphi_{c,2} = \varphi_c + \Phi, \quad (3)$$

where Φ is the flux enclosed in the loop terminated by $S_{c,1}$ and $S_{c,2}$.

2. Double 0D quantum dots

Now, we present the Hamiltonians of double 0D quantum dots.

We start with the Hamiltonian of a single 0D quantum dot D_x at location \mathbf{x} :

$$\mathcal{H}_{D_x,0D} = \varepsilon_x \sum_{\sigma_z} c_{D_x,\sigma_z}^+ c_{D_x,\sigma_z}, \quad (4)$$

where ε_x is the on-site energy. Similarly, the double quantum dot (D_x, D_y) is characterized by the on-site energies ε_x and ε_y with tunneling amplitude $\Sigma^{(0)}$ between them:

$$\mathcal{H}_{D_y,0D} = \varepsilon_y \sum_{\sigma_z} c_{D_y,\sigma_z}^+ c_{D_y,\sigma_z} \quad (5)$$

$$\mathcal{H}_{T,0} = -\Sigma^{(0)} \sum_{\sigma_z} c_{D_x,\sigma_z}^+ c_{D_y,\sigma_z} + h.c. \quad (6)$$

At the exception of one of the numerical calculations presented in section V, we use $\varepsilon_x = \varepsilon_y = 0$ in the paper, thus with

$$\mathcal{H}_{D_x,0D} = 0 \quad (7)$$

$$\mathcal{H}_{D_y,0D} = 0. \quad (8)$$

3. Normal leads

Now, we present the Hamiltonian of a normal lead.

The Hamiltonian of a normal lead is given by

$$\mathcal{H}_N = -W \sum_{\langle i,j \rangle} \sum_{\sigma_z=\uparrow,\downarrow} \left(c_{i,\sigma_z}^+ c_{j,\sigma_z} + c_{j,\sigma_z}^+ c_{i,\sigma_z} \right), \quad (9)$$

where the normal lead chemical potential is vanishingly small, and the hopping amplitude W is identical to Eq. (1).

B. Model Hamiltonians

Now, we present the Hamiltonians of the devices that will be considered in the paper.

Our previous paper I [51] was based on perturbation theory in the tunnel amplitudes between a 2D metal and four superconducting leads, in the $V = 0^+$ adiabatic limit. In this paper I, the poles of the Green's functions are at the gap edge singularities and those perturbative calculations do not yield small voltage scales in the quartet critical current-voltage characteristics. In our previous paper II, we addressed the connection between the quartet critical current and the Floquet spectra in a situation where 0D quantum dot is connected to four superconducting leads. We then obtained reduction of the quartet critical current at the bias voltage resonance values. Compared to this paper II, the here considered four-terminal double quantum dot Josephson junction is additionally connected to normal lead.

In this section, we provide the Hamiltonians of the three considered models. Subsection II B 1 deals with a multilevel quantum dot connected to four superconducting and to normal leads. Subsections II B 2 and II B 3 deal with two simple models of double 0D quantum dots, also attached to superconducting and normal leads. Subsections II B 2 and II B 3 correspond to “double 0D quantum dot connected to normal lead”, in parallel or in series respectively. The interest of double 0D quantum dots with respect to single 0D quantum dots is explained in the forthcoming subsection II B 4.

1. Multilevel quantum dot

Now, we consider the Hamiltonian of a multilevel quantum dot connected to superconducting and normal leads. We also provide a physical discussion.

We assume that the multilevel quantum dot on figure 2 is intermediate between the short- and long-junction limits, i.e. it has dimension $\gtrsim 2\xi_0$, where $\xi_0 = \hbar v_F / \Delta$ is the BCS coherence length, with v_F the Fermi velocity. Thus, more than two ABS are formed at equilibrium.

The Hamiltonian: We consider finite-size discrete levels on the multilevel quantum dot of figure 2, at the energies Ω_ψ . The corresponding Hamiltonian takes the form

$$\mathcal{H}_{multi} = \sum_\psi \Omega_\psi \sum_{\sigma_z} c_{\psi,\sigma_z}^+ c_{\psi,\sigma_z}, \quad (10)$$

where c_{ψ,σ_z}^+ creates a fermion with spin- σ_z in the state $|\psi\rangle$. The superconducting leads S_a , S_b , $S_{c,1}$ and $S_{c,2}$ are described by the BCS Hamiltonian given by Eq. (1). The normal lead is described by Eq. (9). Tunneling between the leads ($S_a, S_b, S_{c,1}, S_{c,2}$) biased at $(V, -V, 0, 0)$ and the multilevel quantum dot is described by multi-channel contacts at the

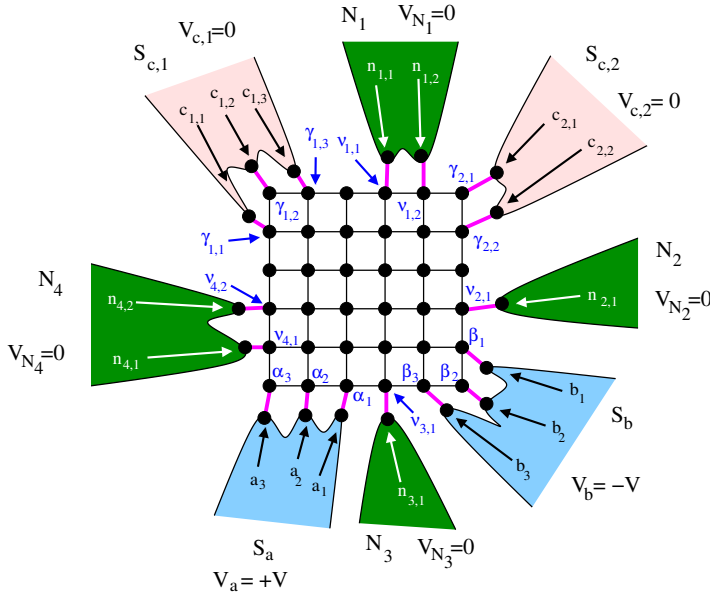


FIG. 2. *The four-terminal superconducting multilevel quantum dot:* The figure shows a multilevel quantum dot connected to the four superconducting leads S_a , S_b , $S_{c,1}$ and $S_{c,2}$ biased at $V_{a,b} = \pm V$ and $V_{c,1} = V_{c,2} = 0$, and to the four grounded normal leads N_1 , N_2 , N_3 and N_4 . The tunneling between the multilevel quantum dot and the superconducting leads is provided in Eqs. (11)-(14). The tunneling to the normal leads is provided in Eq. (15). This model will be used in the following sections III A, III B 1, III B 2, III C and III D.

time τ :

$$\mathcal{H}_{T,a}(\tau) = -\Sigma_a^{(1)} \exp(-ieV\tau/\hbar) \sum_s \sum_{\sigma_z} c_{a_s, \sigma_z}^+ c_{a_s, \sigma_z} + h.c. \quad (11)$$

$$\mathcal{H}_{T,b}(\tau) = -\Sigma_b^{(1)} \exp(ieV\tau/\hbar) \sum_t \sum_{\sigma_z} c_{b_t, \sigma_z}^+ c_{b_t, \sigma_z} + h.c. \quad (12)$$

$$\mathcal{H}_{T,c_1} = -\Sigma_{c_1}^{(1)} \sum_u \sum_{\sigma_z} c_{c_{1,u}, \sigma_z}^+ c_{\gamma_{1,u}, \sigma_z} + h.c. \quad (13)$$

$$\mathcal{H}_{T,c_2} = -\Sigma_{c_2}^{(1)} \sum_v \sum_{\sigma_z} c_{c_{2,v}, \sigma_z}^+ c_{\gamma_{2,v}, \sigma_z} + h.c., \quad (14)$$

where the integers s, t, u and v label the collection of hopping amplitudes in real space, thus realizing a multichannel interface. As an approximation, the hopping amplitudes in Eqs. (11)-(14) were chosen identical within each contact: $\Sigma_{a,s}^{(1)} \equiv \Sigma_a^{(1)}$, $\Sigma_{b,t}^{(1)} \equiv \Sigma_b^{(1)}$, $\Sigma_{c_1,u}^{(1)} \equiv \Sigma_{c_1}^{(1)}$ and $\Sigma_{c_2,v}^{(1)} \equiv \Sigma_{c_2}^{(1)}$. The contact transparencies are parameterized by $\Gamma_a = (\Sigma_a^{(1)})^2/W$, $\Gamma_b = (\Sigma_b^{(1)})^2/W$, $\Gamma_{c_1} = (\Sigma_{c_1}^{(1)})^2/W$ and $\Gamma_{c_2} = (\Sigma_{c_2}^{(1)})^2/W$. The notations c_{a_s, σ_z}^+ , c_{b_t, σ_z}^+ , $c_{c_{1,u}, \sigma_z}^+$ and $c_{c_{2,v}, \sigma_z}^+$ refer to creating a spin- σ_z fermion at the tight-binding sites labeled by a_s , b_t , $c_{1,u}$ and $c_{2,v}$ belonging to the superconducting leads S_a , S_b , $S_{c,1}$ and $S_{c,2}$, see (a_1, a_2, a_3) , (b_1, b_2) , $(c_{1,1}, c_{1,2}, c_{1,3})$ and $(c_{2,1}, c_{2,2})$ in figure 2. Similarly, c_{a_s, σ_z} , c_{b_t, σ_z} , $c_{\gamma_{1,u}, \sigma_z}$ and $c_{\gamma_{2,v}, \sigma_z}$ destroy a spin- σ_z fermion at the tight-binding sites labeled by α_s , β_t , $\gamma_{1,u}$ and $\gamma_{2,v}$, see $(\alpha_1, \alpha_2, \alpha_3)$, (β_1, β_2) , $(\gamma_{1,1}, \gamma_{1,2}, \gamma_{1,3})$ and $(\gamma_{2,1}, \gamma_{2,2})$ in figure 2.

We assume in addition that q_0 normal leads labeled by $n_q = 1, \dots, q_0$ are connected to the multilevel quantum dot by the following tunneling Hamiltonian:

$$\mathcal{H}_{T,N_q} = -\Sigma_{N_q}^{(1)} \sum_w \sum_{\sigma_z} c_{n_{q,w}, \sigma_z}^+ c_{v_{q,w}, \sigma_z} + h.c., \quad (15)$$

where $n_{q,w}$ is the tight-binding site labeled by w in the lead N_q , and $v_{q,w}$ is its counterpart on the multilevel quantum dot. We

took in Eq. (15) the same tunneling amplitudes $\Sigma_{N_q}^{(1)} \equiv \Sigma_{N_q, w}^{(1)}$ at each contact. For instance, for $q_0 = 4$, the tight-binding sites $(n_{1,1}, n_{1,2}), n_{2,1}, n_{3,1}$ and $(n_{4,1}, n_{4,2})$ belonging to the normal leads N_1 , N_2 , N_3 and N_4 respectively are shown in figure 2, together with their counterparts $(v_{1,1}, v_{1,2}), v_{2,1}, v_{3,1}$ and $(v_{4,1}, v_{4,2})$ in the multilevel quantum dot.

This model will be used in the following sections III A, III B 1, III B 2, III C and III D.

Physical remarks: Two antagonist effects appear:

(i) In absence of coupling to the superconductors, increasing the coupling to the normal leads has the tendency to smoothen the energy-dependence of the local density of states.

(ii) In the presence of coupling to the superconducting leads, the Floquet resonances have the tendency to produce sharp peaks in the local density of states as a function of energy.

Physically, the above item (i) captures the metallic limit of “weak sample-to-sample fluctuations in the quartet critical current”. The item (ii) corresponds to “strong sample-to-sample fluctuations in the quartet current”, where different samples differ by the number of channels at the contacts, or by fluctuations in the shape of the multilevel quantum dot. The metallic limit (i) is ruled out for compatibility with the experiment in Ref. 61, because it does not produce small voltage scales. This is why we focus here on the regime (ii) of weak coupling to the normal leads.

We make an additional assumption about the spectrum $\{\Omega_\psi\}$ of the multilevel quantum dot, see Eq. (10). Namely, we assume pairs of levels at opposite energies, i.e. there are values ψ_1, ψ_2 of the label ψ such that $\Omega_{\psi_1} = -\Omega_{\psi_2}$. Then, two-Cooper pair resonance emerges at specific values of the bias voltage, such as $2eV_* = \Omega_{\psi_1} - \Omega_{\psi_2} = 2\Omega_{\psi_1}$ in the limit of weak coupling.

Now, we simplify the multilevel quantum dot into phenomenological models of double 0D quantum dots that seem to be the “minimal models” for the two-Cooper pair resonance.

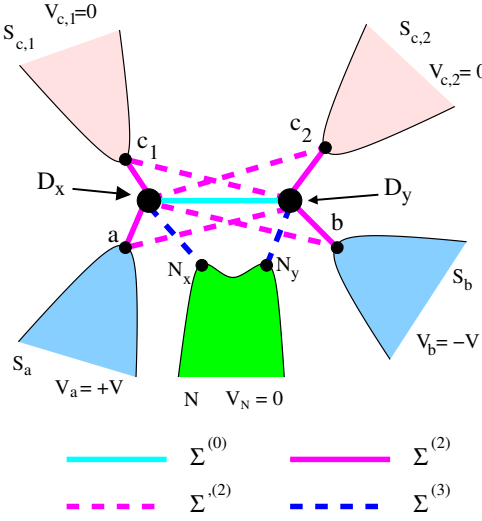


FIG. 3. The four-terminal phenomenological model of superconducting double 0D quantum dot with normal lead in parallel: The figure shows a double 0D quantum dot connected to the four superconducting leads $S_a, S_b, S_{c,1}$ and $S_{c,2}$ biased at $V_{a,b} = \pm V$ and $V_{c,1} = V_{c,2} = 0$, and to the four grounded normal leads N_1, N_2, N_3 and N_4 . The corresponding Hamiltonian is provided in section II B 2. The coupling $\Sigma^{(0)}$ directly couples the two quantum dots D_x and D_y , see Eq. (6). The “direct” coupling $\Sigma^{(2)}$ connects D_x to S_a , D_x to $S_{c,1}$, D_y to S_b and D_y to $S_{c,2}$, see Eqs. (16)-(20). The “crossed” coupling $\Sigma^{(2)}$ connects D_x to S_b , D_x to $S_{c,2}$, D_y to S_a and D_y to $S_{c,1}$, see Eqs. (21)-(25). The coupling $\Sigma^{(3)}$ connects the 0D quantum dot D_x to N_x and D_y to N_y , where N_x and N_y are the two tight-binding sites on the normal lead N -side of the contacts, see Eqs. (26)-(28). This model will be used in the following sections III A, III B 1, III B 2, III B 3, III C and III D and III E.

2. Phenomenological model of double 0D quantum dot with normal lead in parallel

Now, we present the Hamiltonian of a double 0D quantum dot with normal lead in parallel, and additionally connected to superconducting leads. We also provide a physical discussion.

The Hamiltonian: We consider a second model, i.e. a “phenomenological model of double 0D quantum dot with normal lead in parallel”, see figure 3. The quantum dots D_x and D_y have the vanishingly small Hamiltonians of Eqs. (7) and (8). The coupling between D_x and D_y is given by Eq. (6) with the hopping amplitude $\Sigma^{(0)}$ shown as a light blue line in figure 3. Again, the superconducting leads $S_a, S_b, S_{c,1}$ and $S_{c,2}$ are described by the BCS Hamiltonian, see Eq. (1). Tunneling between the leads $S_a, S_b, S_{c,1}$ and $S_{c,2}$ and the double 0D quan-

tum dot (D_x, D_y) is described by single-channel contacts:

$$\mathcal{H}_{T,D_x,a}(\tau) = -\Sigma_{D_x,a}^{(2)} \exp(-ieV\tau/\hbar) \sum_{\sigma_z} c_{a,\sigma_z}^+ c_{D_x,\sigma_z} + h.c. \quad (16)$$

$$\mathcal{H}_{T,D_y,b}(\tau) = -\Sigma_{D_y,b}^{(2)} \exp(ieV\tau/\hbar) \sum_{\sigma_z} c_{b,\sigma_z}^+ c_{D_y,\sigma_z} + h.c. \quad (17)$$

$$\mathcal{H}_{T,D_x,c_1} = -\Sigma_{D_x,c_1}^{(2)} \sum_{\sigma_z} c_{c_1,\sigma_z}^+ c_{D_x,\sigma_z} + h.c. \quad (18)$$

$$\mathcal{H}_{T,D_y,c_2} = -\Sigma_{D_y,c_2}^{(2)} \sum_{\sigma_z} c_{c_2,\sigma_z}^+ c_{D_y,\sigma_z} + h.c., \quad (19)$$

and we assume

$$\Sigma_{D_x,a}^{(2)} = \Sigma_{D_y,b}^{(2)} = \Sigma_{D_x,c_1}^{(2)} = \Sigma_{D_y,c_2}^{(2)} \equiv \Sigma^{(2)}. \quad (20)$$

We parameterize the contact transparency with $\Gamma = (\Sigma^{(2)})^2/W$.

In addition, we include the following “crossed tunneling terms” between D_x and S_b , $S_{c,2}$ and between D_y and S_a , $S_{c,1}$:

$$\mathcal{H}_{T,D_x,b}(\tau) = -\Sigma_{D_x,b}^{(2)} \exp(ieV\tau/\hbar) \sum_{\sigma_z} c_{b,\sigma_z}^+ c_{D_x,\sigma_z} + h.c. \quad (21)$$

$$\mathcal{H}_{T,D_y,a}(\tau) = -\Sigma_{D_y,a}^{(2)} \exp(-ieV\tau/\hbar) \sum_{\sigma_z} c_{a,\sigma_z}^+ c_{D_y,\sigma_z} + h.c. \quad (22)$$

$$\mathcal{H}_{T,D_x,c_2} = -\Sigma_{D_x,c_2}^{(2)} \sum_{\sigma_z} c_{c_2,\sigma_z}^+ c_{D_x,\sigma_z} + h.c. \quad (23)$$

$$\mathcal{H}_{T,D_y,c_1} = -\Sigma_{D_y,c_1}^{(2)} \sum_{\sigma_z} c_{c_1,\sigma_z}^+ c_{D_y,\sigma_z} + h.c., \quad (24)$$

and we assume

$$\Sigma_{D_x,b}^{(2)} = \Sigma_{D_y,a}^{(2)} = \Sigma_{D_x,c_2}^{(2)} = \Sigma_{D_y,c_1}^{(2)} \equiv \Sigma'^{(2)}. \quad (25)$$

We parameterize the crossed contact transparency with $\Gamma' = (\Sigma'^{(2)})^2/W$.

The Hamiltonian of the normal lead is given by Eq. (9). Tunneling between the quantum dots D_x, D_y and the normal lead N is realized with the single-channel contacts (D_x, N_x) and (D_y, N_y) :

$$\mathcal{H}_{T,D_x,N_x} = -\Sigma_{D_x,N_x}^{(3)} \sum_{\sigma_z} c_{N_x,\sigma_z}^+ c_{D_x,\sigma_z} + h.c. \quad (26)$$

$$\mathcal{H}_{T,D_y,N_y} = -\Sigma_{D_y,N_y}^{(3)} \sum_{\sigma_z} c_{N_y,\sigma_z}^+ c_{D_y,\sigma_z} + h.c., \quad (27)$$

N_x and N_y being tight-binding sites belonging to the normal lead, and connected to D_x and D_y respectively by Eqs. (26)-(27). We additionally assume that $\Sigma_{D_x,N_x}^{(3)}$ and $\Sigma_{D_y,N_y}^{(3)}$ are identical:

$$\Sigma_{D_x,N_x}^{(3)} = \Sigma_{N_x,D_x}^{(3)} = \Sigma_{D_y,N_y}^{(3)} = \Sigma_{N_y,D_y}^{(3)} \equiv \Sigma^{(3)}. \quad (28)$$

This model will be used in the following sections III A, III B 1, III B 2, III B 3, III C and III D and III E.

Physical remarks: Once disconnected from the superconducting or normal leads, this phenomenological model of double 0D quantum dot with normal lead in parallel naturally

yields the pair of opposite-energy levels that is relevant to the two-Cooper pair resonance.

Now, we consider in section II B 3 another phenomenological model that includes the possibility of quartet current oscillating at the scale of the Fermi wave-length as a function a dimension of the device.

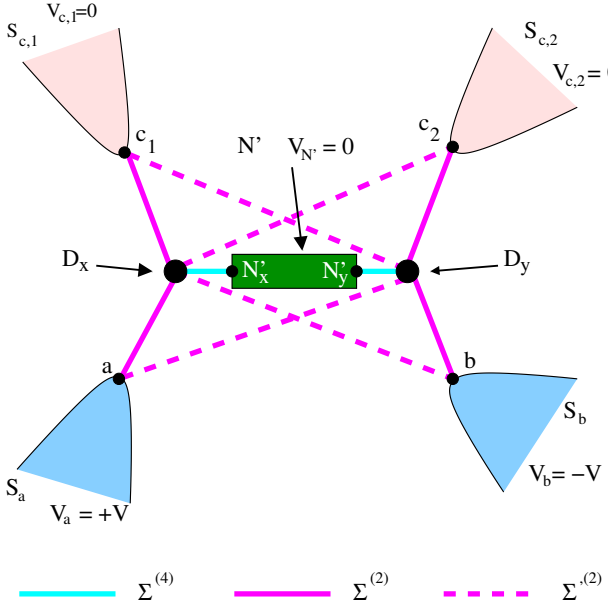


FIG. 4. *The four-terminal phenomenological model of superconducting double 0D quantum dot with normal lead in series:* The figure shows a double 0D quantum dot connected to the four superconducting leads $S_a, S_b, S_{c,1}$ and $S_{c,2}$ biased at $V_{a,b} = \pm V$ and $V_{c,1} = V_{c,2} = 0$, and to the four grounded normal leads N_1, N_2, N_3 and N_4 . The corresponding Hamiltonian is provided in section II B 3. The coupling $\Sigma^{(4)}$ [see Eqs. (29)-(31)] couples the two quantum dots D_x and D_y to the conductor N' that, in the calculations, is characterized by the local and nonlocal Green's functions among the tight-binding sites N_x and N_y . The “direct” coupling $\Sigma^{(2)}$ connects D_x to S_a , D_x to $S_{c,1}$, D_y to S_b and D_y to $S_{c,2}$, see Eqs. (16)-(20). The “crossed” coupling $\Sigma'^{(2)}$ connects D_x to S_b , D_x to $S_{c,2}$, D_y to S_a and D_y to $S_{c,1}$, see Eqs. (21)-(25). This model will be used in the following sections III B 1, III B 2, III B 3, III C, III E and V. .

3. Phenomenological model of double 0D quantum dot with normal lead in series

Now, we consider the Hamiltonian of a double 0D quantum dot with normal lead in series, and connected to superconducting leads. We also provide a physical discussion.

The Hamiltonian: Namely, we consider a third model, i.e. a “phenomenological model of double 0D quantum dot with normal lead in series” connected by single-channel contacts through a 2D metal, see figure 4. The difference with the previous section II B 2 is in the coupling to the normal lead.

As in the above section II B 2, the quantum dots D_x and D_y have the vanishingly small Hamiltonians of Eqs. (7) and (8), the superconducting leads $S_a, S_b, S_{c,1}$ and $S_{c,2}$ are described by the BCS Hamiltonian given by Eq. (1) and the normal lead

is described by Eq. (9). Tunneling between the leads $S_a, S_b, S_{c,1}$ and $S_{c,2}$ and the double quantum dot (D_x, D_y) is described by the same single-channel contacts as in the above Eqs. (16)-(19). In addition, the crossed tunneling amplitudes given by Eqs. (21)-(24) are also included for completeness.

The coupling to the normal lead is phenomenologically accounted for by replacing the tunneling amplitude $\Sigma^{(0)}$ between the quantum dots by propagation through the normal conductor N' connected to the dots D_x and D_y by the single-channel tunneling amplitudes $\Sigma_{D_x, N'_x}^{(0)}$ and $\Sigma_{D_y, N'_y}^{(0)}$ respectively:

$$\mathcal{H}_{T, D_x, N'_x} = -\Sigma_{D_x, N'_x}^{(4)} \sum_{\sigma_z} c_{N'_x, \sigma_z}^+ c_{D_x, \sigma_z} + h.c. \quad (29)$$

$$\mathcal{H}_{T, D_y, N'_y} = -\Sigma_{D_y, N'_y}^{(4)} \sum_{\sigma_z} c_{N'_y, \sigma_z}^+ c_{D_y, \sigma_z} + h.c., \quad (30)$$

where we assume

$$\Sigma_{D_x, N'_x}^{(4)} = \Sigma_{N'_x, D_x}^{(4)} = \Sigma_{D_y, N'_y}^{(4)} = \Sigma_{N'_y, D_y}^{(4)} \equiv \Sigma^{(4)}. \quad (31)$$

The normal conductor N' is characterized by the local Green's functions at N'_x or N'_y , in addition to nonlocal ones from N'_x to N'_y or from N'_y to N'_x across N' . The nonlocal Green's function between N'_x and N'_y generally has to be a complex number.

This model will be used in the following sections III B 1, III B 2, III B 3, III C, III E and V.

Physical remarks: Within this phenomenological model of double 0D quantum dot with normal lead in series, the quartet critical current at resonance is sensitive to the Green's function connecting the two quantum dots D_x and D_y . This Green's function is itself sensitive to the microscopic details of the model, i.e. on the value of the separation R_0 between the tight-binding sites N'_x and N'_y within the interval $[R'_0 - \lambda_F/2, R'_0 + \lambda_F/2]$, where λ_F is the Fermi wave-length. Thus, this phenomenological model of double 0D quantum dot with normal lead in series produces strong sample-to-sample fluctuations of the quartet current, where different samples correspond to different values of R_0 .

Once disconnected from the superconducting or normal leads, this phenomenological model of double 0D quantum dot with normal lead in series also yields the pair of opposite-energy levels that is central to the two-Cooper pair resonance.

In section V, we present numerical results for this model in the regime of strong sample-to-sample fluctuations.

4. Comments on the choice of a model

Now, we explain why we focus on the double quantum dot Hamiltonians presented in the above subsections II B 2 and II B 3, instead of a single, three or four-quantum dot Hamiltonians.

First, we comparatively examine single and double 0D quantum dots.

At equilibrium, the ABS of a single 0D quantum dot have energy scale Γ typically set by $\Gamma = \Sigma^2/W$, where Σ is the tunneling amplitude between the dot and the superconducting leads. It turns out that, at small Γ , the quasiadiabatic regime

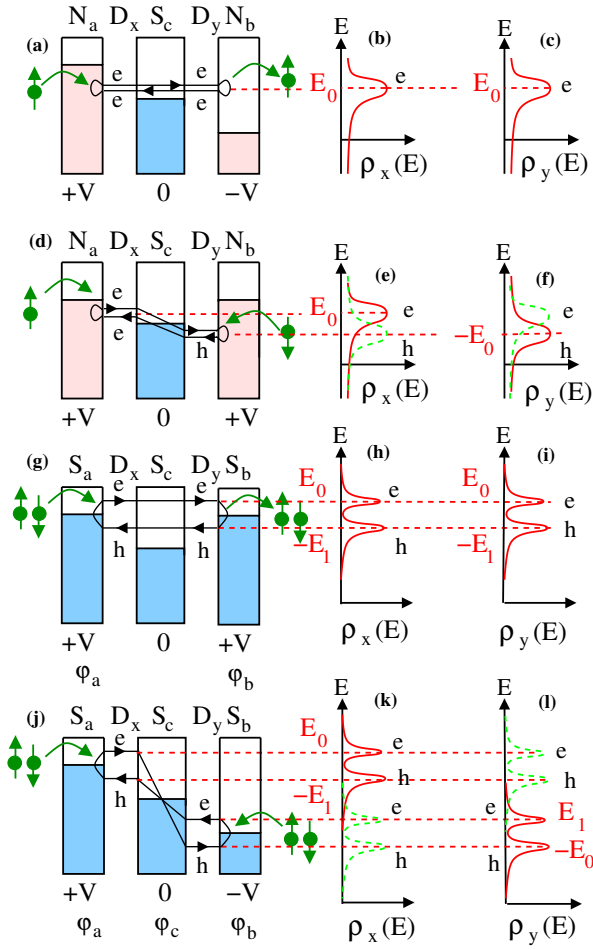


FIG. 5. *The nonlocal resonances in three-terminal devices.* Panels a, d, g and j show the lowest-order diagrams of elastic cotunneling (EC), crossed Andreev reflection (CAR), double elastic cotunneling (dEC) and double crossed Andreev reflection (dCAR) respectively. Panels b, e, h and k show the energy- E -dependence of the density of states $\rho_x(E)$ on the quantum dot D_x and panels c, f, i and l show the corresponding $\rho_y(E)$ on the quantum dot D_y . Panels e, f, k and l also show for completeness by green dashed lines the complementary resonances that do not directly contribute to the corresponding transport processes.

$V \lesssim V_*$ with $eV_* \sim \Gamma$, does not produce enhanced quartet critical current according to the forthcoming subsection III C where the two-Cooper pair resonance is put in correspondence with nonadiabatic effects.

At equilibrium, double 0D quantum dots are characterized by levels at the opposite energies $\pm\Omega$, where Ω is set by the tunneling amplitude $\Sigma^{(0)}$ between the dots, see Eq. (6). Then, the voltage energy $eV_* = \Omega$ of the first resonance remains finite in the weak-coupling limit, which implies nonadiabatic behavior and enhancement of the quartet critical current at low V if Ω is small compared to the superconducting gap Δ .

Double 0D quantum dots are thus better candidates than single 0D quantum dots to produce large quartet critical current at small bias voltage because the two-Cooper pair resonance is also there in the weak-coupling regime of small- Γ .

The interest of double 0D quantum dots is also related to the observation that the corresponding four energy levels can accommodate the four fermions of a quartet as a “real state”, see subsection III E and Appendix A. In this sense, the double 0D quantum dots have the “minimal complexity” in comparison with three- or four-quantum dot devices.

III. MECHANISM FOR THE TWO-COOPER PAIR RESONANCE

In this section, we present a general mechanism for emergence of the two-Cooper pair resonance. We start in subsection III A with an introduction to the three-terminal N_a -dot- S_c -dot- N_b Cooper pair beam splitters, and to S_a -dot- S_c -dot- S_b three-terminal Josephson junctions. Next, we calculate effective non-Hermitian self-energies and Hamiltonians in subsection III B. The transport formula are discussed in subsection III C in connection with emergence of resonances. Current conservation is discussed in subsection III D. Finally, in subsection III E, we demonstrate stability in the time-evolution of a quartet created at time $t = 0$, in the limit of weak coupling.

A. Three-terminal two-Cooper pair resonance

In this subsection, we present an introduction to the two-Cooper pair resonance in three-terminal Josephson junctions, i.e. in S_a -dot- S_c -dot- S_b devices, starting with nonlocal resonances in the three-terminal N_a -dot- S_c -dot- N_b .

Figures 5a, 5b and 5c show the condition for nonlocal resonance of elastic cotunneling (EC) [2–15] in N_a -dot- S_c -dot- N_b Cooper pair beam splitters. EC transfers single-particle states from N_a to N_b across S_c , and contributes to negative nonlocal conductance $\mathcal{G}_{a,b} = \partial I_a / \partial V_b$ on the voltage biasing condition $V_a = -V_b$, where I_a is the current transmitted into the normal lead N_a . EC is resonant if both quantum dots D_x and D_y have levels at the same energy $\varepsilon_x = \varepsilon_y$, where $\omega = \varepsilon_x = \varepsilon_y$ is the energy of the incoming electron in figure 5a.

Figures 5d, 5e, 5f show CAR [2–15] in N_a -dot- S_c -dot- N_b Cooper pair beam splitters, which reflects by nonlocal Andreev reflection spin-up electron impinging from N_a as spin-down hole transmitted into N_b , leaving a Cooper pair in the central S_c . CAR contributes for positive value to the nonlocal conductance $\mathcal{G}_{a,b}$ at the bias voltages $V_a = V_b$ and $V_c = 0$. The nonlocal CAR resonance is obtained if the quantum dots D_x and D_y have levels at the opposite energies $\varepsilon_x = -\varepsilon_y \equiv \omega$.

Considering S_a -dot- S_c -dot- S_b three-terminal Josephson junctions, figures 5g, 5h, 5i feature double elastic cotunneling (dEC) [5, 7, 10], which transfers Cooper pairs from S_a to S_b across S_c at the bias voltages $V_a = V_b$. This process is resonant if $\omega = E_0$ (for the spin-up electron crossing D_x or D_y) and $-\omega + 2eV = -E_1$ (for the spin-down hole crossing D_x or D_y). Thus, dEC is resonant if $eV = (E_0 - E_1)/2$ and $\omega = E_0$.

Concerning double crossed Andreev reflection (dCAR) in S_a -dot- S_c -dot- S_b three-terminal Josephson junctions in figures 5j, 5k and 5l, two Cooper pairs from S_a and S_b biased at the

voltages $\pm V$ cooperatively enter the grounded S_c , producing transient correlations among four fermions, i.e. the so-called quartets. Then,

$$\omega = E_0 \quad (32)$$

$$-\omega + 2eV = -E_1 \quad (33)$$

are obtained at resonance. Conversely, the same Eqs. (32)-(33) are obtained for resonance of the spin-up electron and spin-down holes crossing D_y .

Now, we assume that D_x and D_y are gathered into a single multilevel quantum dot. Assuming the opposite energies $E_0 = -E_1 \equiv \Omega$ implies $\omega = \Omega$ and $-\omega + 2eV = \Omega$, which yields

$$eV = \omega = \Omega \quad (34)$$

for the nonlocal quartet resonance.

Overall, the argument leading to Eq. (34) confirms that non-local quartet resonance is produced at voltage energy eV that can be much smaller than the superconducting gap Δ , if the energy scales $\pm \Omega$ are also within $\pm \Delta$, see also the preceding subsection II B 4.

B. Effective non-Hermitian self-energy and Hamiltonian

In this subsection, we present how effective non-Hermitian self-energies or Hamiltonians can be obtained in the infinite-gap limit from the models presented in the above section II.

We start in section III B with the Dyson equations for the three models presented in the above subsections II B 1, II B 2 and II B 3. Emergence of non-Hermitian self-energy in the infinite-gap limit is discussed in subsection III B 2. Non-Hermitian Hamiltonians are next presented for double quantum dots in the infinite-gap limit, see subsection III B 3.

1. Closing the Dyson equations

In this subsection, we provide the starting-point Dyson equations. We adopt a general viewpoint on the three models of subsections II B 1, II B 2 and II B 3, i.e. multilevel quantum dots, double 0D quantum dots connected in parallel and in series respectively, see also figures 2, 3 and 4.

The “quantum dot D ” is coupled to p_0 superconducting leads labeled by $n_p = 1, \dots, p_0$ and to q_0 normal leads labeled by $n_q = 1, \dots, q_0$, where $p_0 = q_0 = 4$ are used in figure 2. The Dyson equations take the form

$$\begin{aligned} \hat{G}_{D,D} &= \hat{g}_{D,D} + \sum_{n_q=1}^{q_0} \sum_{n_{q'}=1}^{q_0} \hat{g}_{D,D} \hat{\Sigma}_{D,N_{n_q}}^{(5)} \hat{g}_{N_{n_q},N_{n_{q'}}} \hat{\Sigma}_{N_{n_{q'}},D}^{(5)} \hat{G}_{D,D} \\ &+ \sum_{n_p=1}^{p_0} \hat{g}_{D,D} \hat{\Sigma}_{D,S_{n_p}}^{(5)} \hat{g}_{S_{n_p},S_{n_p}} \hat{\Sigma}_{S_{n_p},D}^{(5)} \hat{G}_{D,D}. \end{aligned} \quad (35)$$

The notation “ D ” in Eq. (35) refers to the collection of the tight-binding sites in absence of coupling to the superconducting or normal leads, and to the direct coupling between them. For instance, D represents finite-size tight-binding multilevel

quantum dot, see subsection II B 1, or D_x - D_y double quantum dot, see subsections II B 2 and II B 3. The notation $\Sigma^{(5)}$ denotes generic hopping amplitude, with the normal lead N_{n_q} (corresponding to $\hat{\Sigma}_{D,N_{n_q}}^{(5)} = \hat{\Sigma}_{N_{n_q},D}^{(5)}$), or with the superconducting lead S_{n_p} (corresponding to $\hat{\Sigma}_{D,S_{n_p}}^{(5)} = \hat{\Sigma}_{S_{n_p},D}^{(5)}$).

The notations $\hat{g}_{N_{n_q},N_{n_{q'}}}$ and $\hat{g}_{S_{n_p},S_{n_p}}$ stand for the bare Green’s functions of the normal or superconducting leads N_{n_q} , $N_{n_{q'}}$ or S_{n_p} respectively, and $\hat{g}_{D,D}$, $\hat{G}_{D,D}$ are the bare and fully dressed quantum dot Green’s functions. The bare Green’s functions are given by

$$\hat{g}_{D,D,x,y}^{A,1,1} = \sum_{\psi} \langle \mathbf{x} | \psi \rangle \frac{1}{\omega - \varepsilon_{\psi} - i\eta} \langle \psi | \mathbf{y} \rangle \quad (36)$$

$$\hat{g}_{D,D,x,y}^{A,2,2} = \sum_{\psi} \langle \mathbf{x} | \psi \rangle \frac{1}{\omega + \varepsilon_{\psi} - i\eta} \langle \psi | \mathbf{y} \rangle, \quad (37)$$

where “1, 1” and “2, 2” refer to the electron-electron and hole-hole channels respectively. In addition, $\hat{g}_{D,D,x,y}^{A,1,2} = \hat{g}_{D,D,x,y}^{A,2,1} = 0$ because of the absence of superconducting pairing on the quantum dot. The Dynes parameter η in Eqs. (36)-(37) [85–88] makes the distinction between the advanced and retarded Green’s functions, and it can be used to capture relaxation on the quantum dot [47]. As in the previous Eq. (10), the notation $|\psi\rangle$ in Eqs. (36)-(37) stands for the single-particle states, and $\langle \mathbf{x} | \psi \rangle$, $\langle \mathbf{y} | \psi \rangle$ are the corresponding wave-functions at the tight-binding sites \mathbf{x} and \mathbf{y} .

The bare and fully dressed Green’s functions $\hat{g}_{D,D}$ and $\hat{G}_{D,D}$ have entries in the Nambu labels, and in the tight-binding sites making the contacts between the dot and the normal or superconducting leads N_{n_q} or S_{n_p} . In addition, those matrices have entries in the set of the harmonics of the Josephson frequency.

2. Effective non-Hermitian self-energy

In this subsection, we explain how effective non-Hermitian self-energy is obtained in the infinite-gap limit. The infinite-gap limit was introduced and considered over the last few years, see for instance Refs. 81, 91, and 92 to cite but a few.

Specifically, Eq. (35) is rewritten as

$$\begin{aligned} & \left[\hat{g}_{D,D}^{-1}(\omega) - \sum_{n_q=1}^{q_0} \sum_{n_{q'}=1}^{q_0} \hat{\Sigma}_{D,N_{n_q}}^{(5)} \hat{g}_{N_{n_q},N_{n_{q'}}} \hat{\Sigma}_{N_{n_{q'}},D}^{(5)} \right. \\ & \left. - \sum_{n_p=1}^{p_0} \hat{\Sigma}_{D,S_{n_p}}^{(5)} \hat{g}_{S_{n_p},S_{n_p}} \hat{\Sigma}_{S_{n_p},D}^{(5)} \right] \hat{G}_{D,D}(\omega) = \hat{I}. \end{aligned} \quad (38)$$

In addition, $\hat{g}_{S,S}$ is independent on ω in the considered infinite-gap limit, and the local Green’s function $\hat{g}_{N_{n_q},N_{n_{q'}}}$ in the normal leads is also taken as being independent on energy.

Then, Eq. (38) can be rewritten as

$$[\omega - \hat{\Sigma}_{NonHer.}(\omega)]^{-1} \hat{G}_{D,D}(\omega) = \hat{I}, \quad (39)$$

where the self-energy

$$\begin{aligned}\hat{\Sigma}_{NonHer.}(\omega) &= \omega - \hat{g}_{D,D}^{-1}(\omega) \\ &+ \sum_{n_q=1}^{q_0} \sum_{n_{q'}=1}^{q_0} \hat{\Sigma}_{D,N_{n_q}}^{(5)} \hat{g}_{N_{n_q},N_{n_{q'}}} \hat{\Sigma}_{N_{n_{q'}},D}^{(5)} \\ &+ \sum_{n_p=1}^{p_0} \hat{\Sigma}_{D,S_{n_p}}^{(5)} \hat{g}_{S_{n_p},S_{n_p}} \hat{\Sigma}_{S_{n_p},D}^{(5)}\end{aligned}\quad (40)$$

in non-Hermitian, due to $\hat{g}_{N_{n_q},N_{n_{q'}}}$.

3. Specializing to double quantum dots

In this subsection, we discuss emergence of non-Hermitian Hamiltonian for the phenomenological model of double 0D quantum dots. The normal leads in parallel, see subsection II B 2, are treated in the same framework as normal leads in series, see subsection II B 3.

We make use of the same compact notations as in the previous subsections III B 1 and III B 2. Then we show that the effective non-Hermitian self-energy $\hat{\Sigma}_{NonHer.}(\omega)$ in Eq. (40) becomes energy-independent for those double 0D quantum dots, thus defining the effective non-Hermitian Hamiltonian $\hat{\mathcal{H}}_{eff}^{(\infty)} \equiv \hat{\Sigma}_{NonHer.}$ in the infinite-gap limit.

The matrices in Eq. (38) have entries in the tight-binding sites at the boundary of the quantum dot, where the tunneling self-energy between the dot and the superconducting or normal leads is acting. The boundary is identical to the bulk for the double 0D quantum dots D_x - D_y isolated from the leads. Thus, $g_{D,D}$ takes the value

$$\hat{g}_{D,D}^R = (\omega + i\eta - \hat{\mathcal{H}}_{dot})^{-1}, \quad (41)$$

where $\hat{\mathcal{H}}_{dot}$ is the double 0D quantum dot Hamiltonian. The retarded Green's functions of the double 0D quantum dots with normal leads in parallel, see figure 3, can then be expressed as

$$\hat{G}_{D,D}^R = (\omega + i\eta - \hat{\mathcal{H}}_{eff}^{(\infty)})^{-1}, \quad (42)$$

where the infinite-gap-limit effective Hamiltonian

$$\begin{aligned}\hat{\mathcal{H}}_{eff}^{(\infty)} &= \hat{\mathcal{H}}_{dot} + \sum_{n_q=1}^{q_0} \sum_{n_{q'}=1}^{q_0} \hat{\Sigma}_{D,N_{n_q}}^{(5)} \hat{g}_{N_{n_q},N_{n_{q'}}} \hat{\Sigma}_{N_{n_{q'}},D}^{(5)} \\ &+ \sum_{n_p=1}^{p_0} \hat{\Sigma}_{D,S_{n_p}}^{(5)} \hat{g}_{S_{n_p},S_{n_p}} \hat{\Sigma}_{S_{n_p},D}^{(5)}\end{aligned}\quad (43)$$

is non-Hermitian, due to $\hat{g}_{N_{n_q},N_{n_{q'}}}$.

C. Emergence of resonances in the transport formula

In this subsection, we demonstrate that the current at resonance is inverse-proportional to the damping rate.

Using the same notations as in the previous subsections III B 1, III B 2 and III B 3, the current flowing from the multilevel quantum dot into the superconducting lead S_{n_p} is given by the following energy-integral [93–95]:

$$\begin{aligned}I_{D,S_{n_p}} &= \frac{e}{\hbar} \int d\omega \times \\ &\text{Tr} \left\{ \hat{\sigma}_N^z \left[\hat{\Sigma}_{D,S_{n_p}}^{(5)} \hat{G}_{S_{n_p},D}^{+,-} - \hat{\Sigma}_{S_{n_p},D}^{(5)} \hat{G}_{D,S_{n_p}}^{+,-} \right] \right\},\end{aligned}\quad (44)$$

where the Pauli matrix $\hat{\sigma}_N^z$ is defined as $\hat{\sigma}_N^z = \text{diag}(1, -1)$ on the set of the Nambu labels, which is referred to as the subscript “ N ” for “Nambu”. The bare superconducting Green's functions $\hat{g}_{S_{n_p},S_{n_p}}^{+,-} = 0$ are vanishingly small if the infinite-gap limit is taken, and $\hat{g}_{N_{n_q},N_{n_{q'}}}^{+,-} \neq 0$ is nonvanishingly small in the normal leads, due to the corresponding finite value of the normal density of states.

The two terms $\hat{\Sigma}_{D,S_{n_p}}^{(5)} \hat{G}_{S_{n_p},D}^{+,-}$ and $\hat{\Sigma}_{S_{n_p},D}^{(5)} \hat{G}_{D,S_{n_p}}^{+,-}$ in Eq. (44) can be expanded as follows:

$$\hat{\Sigma}_{D,S_{n_p}}^{(5)} \hat{G}_{S_{n_p},D}^{+,-} = \quad (45)$$

$$\sum_{q,q'} \hat{\Sigma}_{D,S_{n_p}}^{(5)} \left[\hat{I} + \hat{G}^R \hat{\Sigma}^{(5)} \right]_{S_{n_p},N_q} \hat{g}_{N_q,N_{q'}}^{+,-} \left[\hat{I} + \hat{\Sigma}^{(5)} \hat{G}^A \right]_{N_{q'},D} \quad (46)$$

$$\hat{\Sigma}_{S_{n_p},D}^{(5)} \hat{G}_{D,S_{n_p}}^{+,-} = \quad (46)$$

$$\sum_{q,q'} \hat{\Sigma}_{S_{n_p},D}^{(5)} \left[\hat{I} + \hat{G}^R \hat{\Sigma}^{(5)} \right]_{D,N_q} \hat{g}_{N_q,N_{q'}}^{+,-} \left[\hat{I} + \hat{\Sigma}^{(5)} \hat{G}^A \right]_{N_{q'},S_{n_p}},$$

where N_q and $N_{q'}$ run over the interfaces between the quantum dot and the normal lead.

Then, Eqs. (44)–(46) become

$$\begin{aligned}I_{D,S_{n_p}} &= \frac{e}{\hbar} \int d\omega \times \\ &\text{Tr} \left\{ \hat{\sigma}_N^z \left[\hat{\Sigma}_{D,S_{n_p}}^{(5)} \hat{g}_{S_{n_p},S_{n_p}}^R \hat{\Sigma}_{S_{n_p},D}^{(5)} \hat{G}_{D,D}^R \hat{\Gamma}_{D,D}^{+,-N} \hat{G}_{D,D}^A \right. \right. \\ &\quad \left. \left. - \hat{\Sigma}_{S_{n_p},D}^{(5)} \hat{G}_{D,D}^R \hat{\Gamma}_{D,D}^{+,-N} \hat{G}_{D,D}^A \hat{\Sigma}_{D,S_{n_p}}^{(5)} \hat{g}_{S_{n_p},S_{n_p}}^R \right] \right\},\end{aligned}\quad (47)$$

where

$$\hat{\Gamma}_{D,D}^{+,-N} = \sum_{n_q=1}^{q_0} \sum_{n_{q'}=1}^{q_0} \hat{\Sigma}_{D,N_{n_q}}^{(5)} \hat{g}_{N_{n_q},N_{n_{q'}}}^{+,-} \hat{\Sigma}_{N_{n_{q'}},D}^{(5)} \quad (48)$$

is diagonal in Nambu and in Floquet.

The retarded and advanced Green's functions are approximated as [48, 78]

$$\hat{G}_{D,D}^R \simeq \sum_{k',l'} \frac{\hat{R}_{k',l'}^R}{\omega - k'eV - E_{l'} + i\delta_{l'}} \quad (49)$$

$$\hat{G}_{D,D}^A \simeq \sum_{k'',l''} \frac{\hat{R}_{k'',l''}^A}{\omega - k''eV - E_{l''} - i\delta_{l''}}, \quad (50)$$

where k', l', k'', l'' are four integers, $E_{l'}$, $E_{l''}$ and $\delta_{l'}$, $\delta_{l''}$ are the Floquet energies and line-width broadening, and $\hat{R}_{k',l'}^R$, $\hat{R}_{k'',l''}^A$ are the matrix residues. Then, inserting Eqs. (49)–(50)

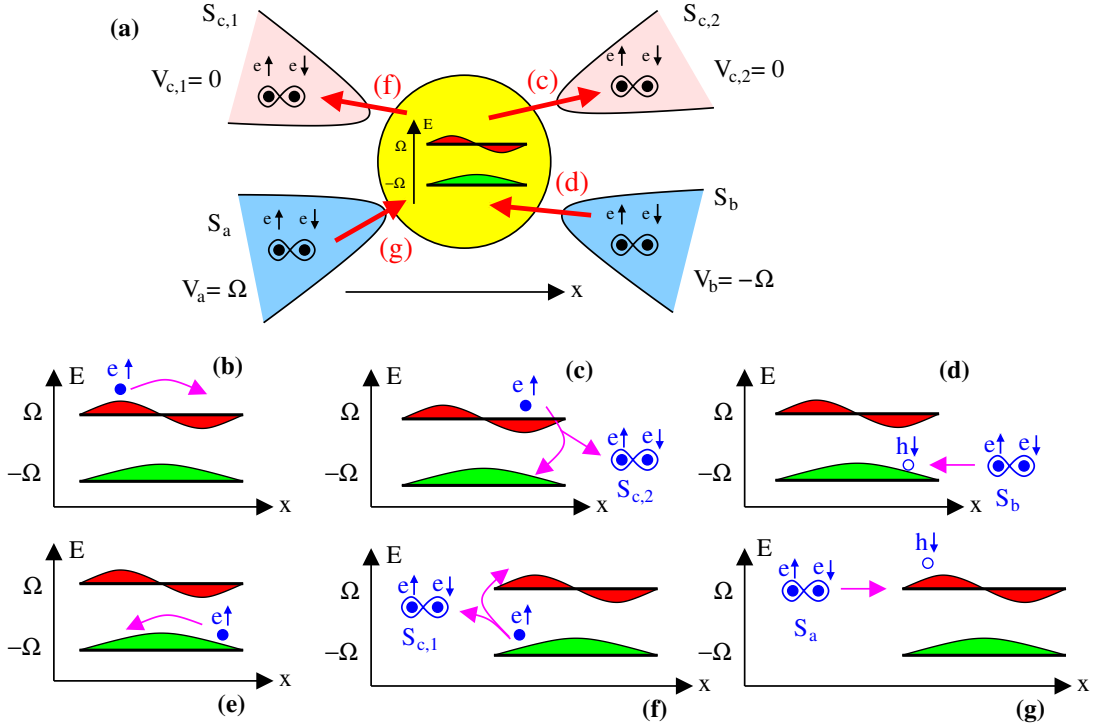


FIG. 6. Panel a schematically shows a quantum dot supporting levels at the opposite energies $E = \pm\Omega$, coupled to the superconducting leads S_a and S_b biased at $eV_{a,b} = \pm\Omega$ and to the grounded $S_{c,1}$ and $S_{c,2}$. Panels b-g represent two levels at the opposite energies $\pm\Omega$, together with the corresponding wave-functions, with absence of node at $E = -\Omega$, and a node at $E = \Omega$. Panels b-g show the time-evolution of the quartet process, involving Cooper pair transmitted into $S_{c,2}$ (panel c), Cooper pair taken from S_b (panel d), Cooper transmitted into $S_{c,1}$ (panel f) and Cooper pair taken from S_a (panel g). Detailed comments about panels b-g are given in the text.

into Eq. (47) and integrating over the energy ω yields

$$I_{D,S_{np}} = \frac{\pi e}{2\hbar} \sum_{(k,l)} \frac{1}{\delta_l} \text{Tr} \left\{ \hat{\sigma}_N^z \times \left[\hat{\Sigma}_{D,S_{np}}^{(5)} \hat{g}_{S_{np},S_{np}} \hat{\Sigma}_{S_{np},D}^{(5)}, \hat{R}_{k,l}^R \hat{\Gamma}_{D,D}^{+, -, N} \hat{R}_{k,l}^A \right]_- \right\}, \quad (51)$$

where $[..., ...]_-$ is a commutator and $\sum_{(k,l)}$ denotes summation over the pairs of labels k and l such that

$$k'eV + E_{l'} = k''eV + E_{l''} \equiv keV + E_l. \quad (52)$$

Thus, we find that the current is inverse proportional to the damping rate set by the parameter δ_l .

D. Current conservation

Now, we note that the effective non-Hermitian Hamiltonian with complex eigenvalues originates from the Hermitian Hamiltonians presented in the above section II. It turns out that the total current is conserved once the fraction of the current transmitted into the normal lead has been taken into account. Current conservation can be demonstrated by assuming that the average number of fermions $\langle \hat{N}_{dot} \rangle$ on the quantum dot is stationary. The Hamiltonian \mathcal{H} can be written as a sum of the Hamiltonians of the quantum dot, of the lead, and tunneling between them. Then, $d\langle \hat{N}_{dot} \rangle / dt = 0$ is equivalent to

current conservation. Thus, non-Hermitian effective Hamiltonian does not contradict current conservation.

E. Evolution in the weak-coupling limit of a quartet created at time $t = 0$

In Appendix A, we demonstrate stability of the quartet created on the double 0D quantum dot at time $t = 0$ in the presence of normal lead coupled in series. This strong ‘‘quartet proximity effect’’ is interpreted as being compatible with the enhanced quartet critical current at the double Cooper pair resonances.

IV. MECHANISM FOR THE INVERSION

We discussed in the previous section III how sharp resonance peaks can appear in the voltage-dependence of the quartet critical current. Now, we provide simple arguments for the magnetic flux- Φ sensitivity of the quartet critical current in the $V = 0^+$ adiabatic limit, focusing on how the quartet critical current $I_{q,c}(\Phi = 0)$ in zero field $\Phi = 0$ compares to $I_{q,c}(\Phi = \pi)$ at half-flux quantum $\Phi = \pi$. Inversion corresponds to larger quartet critical current at $\Phi = \pi$ than at $\Phi = 0$, i.e. $I_{q,c}(\Phi = \pi) > I_{q,c}(\Phi = 0)$. Absence of inversion corresponds to $I_{q,c}(\Phi = \pi) < I_{q,c}(\Phi = 0)$.

Figure 6 shows a sequence of microscopic processes for the quartets in the presence of the two energy levels $E = \pm\Omega$ on the quantum dot. Figure 6b shows spin-up electron at energy $E = \Omega$ on the left-part of the two-level quantum dot, and how it moves to the right-part. Figure 6c shows spin-up electron at energy $E = \Omega$ on the right part of the junction, and how it is converted by Andreev reflection into spin-down hole at energy $E = -\Omega$ at the interface with the $S_{c,2}$ superconducting lead. Figure 6d shows the resulting spin-down hole at energy $E = -\Omega$, together with a Cooper pair taken from S_b . Figure 6e shows the resulting spin-up electron at energy $E = -\Omega$ on the right-part of the quantum dot, and how it moves to the left part. Figure 6f shows spin-up electron at energy $E = -\Omega$ on the left part of the junction, and how it is converted into spin-down hole at energy $E = \Omega$ by Andreev reflection at the interface with $S_{c,1}$. Figure 6g shows the resulting spin-down hole on the left-part of the junction at the energy $E = \Omega$, together with absorption of a Cooper pair taken from S_a , thus coming back to the initial state in figure 6b.

Overall the transition between figures 6b and 6c implies negative sign for the “split quartets” transmitting a Cooper pair into $S_{c,1}$ and another one into $S_{c,2}$, and a positive sign for the “unsplit quartets”, corresponding to two Cooper pairs transmitted into $S_{c,1}$ or into $S_{c,2}$. The resulting opposite signs in the “split” and “unsplit” channels imply the inversion, see our previous paper I [51]. This physical picture for “emergence of inversion in the $V = 0^+$ limit” is confirmed by the calculations presented in Appendix B 2.

Thus, we demonstrated that “inversion between $\Phi = 0$ and $\Phi = \pi$ ” or “absence of inversion” is linked to the quantum dot single-particle wave-functions, i.e. to the number of nodes in their wave-functions.

V. NUMERICAL RESULTS

In this section, we present a selection of the numerical results for the phenomenological model of double 0D quantum dot with normal lead in series, see figure 4 and the Hamiltonian in subsection II B 3. The quantum dots D_x and D_y are coupled to each other by the tunneling amplitude $\Sigma^{(0)}$ defined in Eq. (6). The coupling $\Gamma = \left(\Sigma^{(2)}\right)^2/W$ is defined for hopping between D_x and S_a , D_x and $S_{c,1}$, D_y and S_b , D_y and $S_{c,2}$, see $\Sigma^{(2)}$ in Eq. (20). We add the coupling $\Gamma' = \left(\Sigma'^{(2)}\right)^2/W$ between D_x and S_b , D_x and $S_{c,2}$, D_y and S_a , D_y and $S_{c,1}$, see $\Sigma'^{(2)}$ in Eq. (25). The Green’s functions of N' are given by

$$\hat{g}_{N'_x, N'_y}^{1,1} = \hat{g}_{N'_y, N'_x}^{1,1} = A_R + iA_I \quad (53)$$

$$\hat{g}_{N'_x, N'_y}^{2,2} = \hat{g}_{N'_y, N'_x}^{2,2} = -A_R + iA_I \quad (54)$$

$$\hat{g}_{N'_x, N'_x}^{1,1} = \hat{g}_{N'_y, N'_y}^{1,1} = B_R + iB_I \quad (55)$$

$$\hat{g}_{N'_x, N'_x}^{2,2} = \hat{g}_{N'_y, N'_y}^{2,2} = -B_R + iB_I, \quad (56)$$

where (A_R, A_I) , and (B_R, B_I) are four real-valued parameters for the nonlocal and local Green’s functions $\hat{g}_{N'_x, N'_y} = \hat{g}_{N'_y, N'_x}$ and $\hat{g}_{N'_x, N'_x}, \hat{g}_{N'_y, N'_y}$ respectively, within the assumption $\hat{g}_{N'_x, N'_x} = \hat{g}_{N'_y, N'_y}$.

The assumption of 0D quantum dots implies that the quartet critical current depends on the value of the Green’s function crossing the conductor N' between N'_x and N'_y , see N', N'_x and N'_y in figure 4.

The nonlocal Green’s function crossing N' oscillates with the combinations $\cos(k_F R_0)$ and $\sin(k_F R_0)$, where R_0 is the separation between N'_x and N'_y , and k_F is the Fermi wave-vector. Sharp resonance peaks emerge at fixed $k_F R_0$ in the voltage- V dependence of the quartet current, see the previous section III and the numerical results in the present section. The interplay between those $k_F R_0$ -oscillations in space and the sharp Floquet resonances in the voltage-dependence of the quartet critical current is expected to produce strong log-normal distribution of sample-to-sample fluctuations, where different samples are characterized by different values of R_0 . In this section, we specifically investigate the regime of strong log-normal distribution of sample-to-sample fluctuations and make the physically-motivated assumption that fixing A_R, A_I, B_R and B_I yields quartet critical current-voltage dependence that is qualitatively representative of the signal in this regime of strong sample-to-sample fluctuations.

The codes have been developed over the last few years [46–48, 52, 55, 59, 61, 78]. They are based on recursive calculations as a function of the harmonics of the Josephson frequency [93, 94] (see also the Appendix of Ref. 46) and on sparse matrix algorithms for matrix products. We specifically adapted the code of our recent Ref. 55 to include the local and nonlocal Green’s functions given by Eqs. (53)–(56).

In the forthcoming figures 7 and 8, we present numerical results for the voltage-dependence of the quartet critical current $I_{q,c}$ defined as

$$I_{q,c}(\Phi = 0, eV/\Delta) = \quad (57)$$

$$- \max_{\varphi_q} [I_q(\Phi = 0, \varphi_q, eV/\Delta) - I_q(\Phi = 0, -\varphi_q, eV/\Delta)]$$

$$- \min_{\varphi_q} [I_q(\Phi = 0, \varphi_q, eV/\Delta) - I_q(\Phi = 0, -\varphi_q, eV/\Delta)]$$

$$I_{q,c}(\Phi = \pi, eV/\Delta) = \quad (58)$$

$$- \max_{\varphi_q} [I_q(\Phi = \pi, \varphi_q, eV/\Delta) - I_q(\Phi = \pi, -\varphi_q, eV/\Delta)]$$

$$- \min_{\varphi_q} [I_q(\Phi = \pi, \varphi_q, eV/\Delta) - I_q(\Phi = \pi, -\varphi_q, eV/\Delta)].$$

In addition, we present colormaps for the sign of $I_{q,c}$ as a function of the model parameters (see the forthcoming figures 9 and 10).

Figure 7 shows the normalized bias voltage- eV/Δ -dependence of the quartet critical currents $I_{q,c}(\Phi = 0, eV/\Delta)$ and $I_{q,c}(\Phi = \pi, eV/\Delta)$ at the flux values $\Phi = 0$ and $\Phi = \pi$. The coupling parameters $\Gamma/\Delta = 1$ and $\Gamma'/\Delta = 0$ are used in figure 7.

Figures 7a, 7b and 7c correspond to absence of relaxation with $A_I = 0$, producing small quartet critical current. Figures 7d, 7e, 7f and 7g, 7h, 7i correspond to the nonvanishingly small relaxation parameters $A_I = 0.05/W$ and $A_I = 0.1/W$ respectively, producing large quartet critical current at small voltage ratio eV/Δ . In addition, sharp resonances emerge in the variations of the quartet critical current as a function of eV/Δ for $A_I = 0.05/W$ and $A_I = 0.1/W$ in figures 7d, 7e, 7f

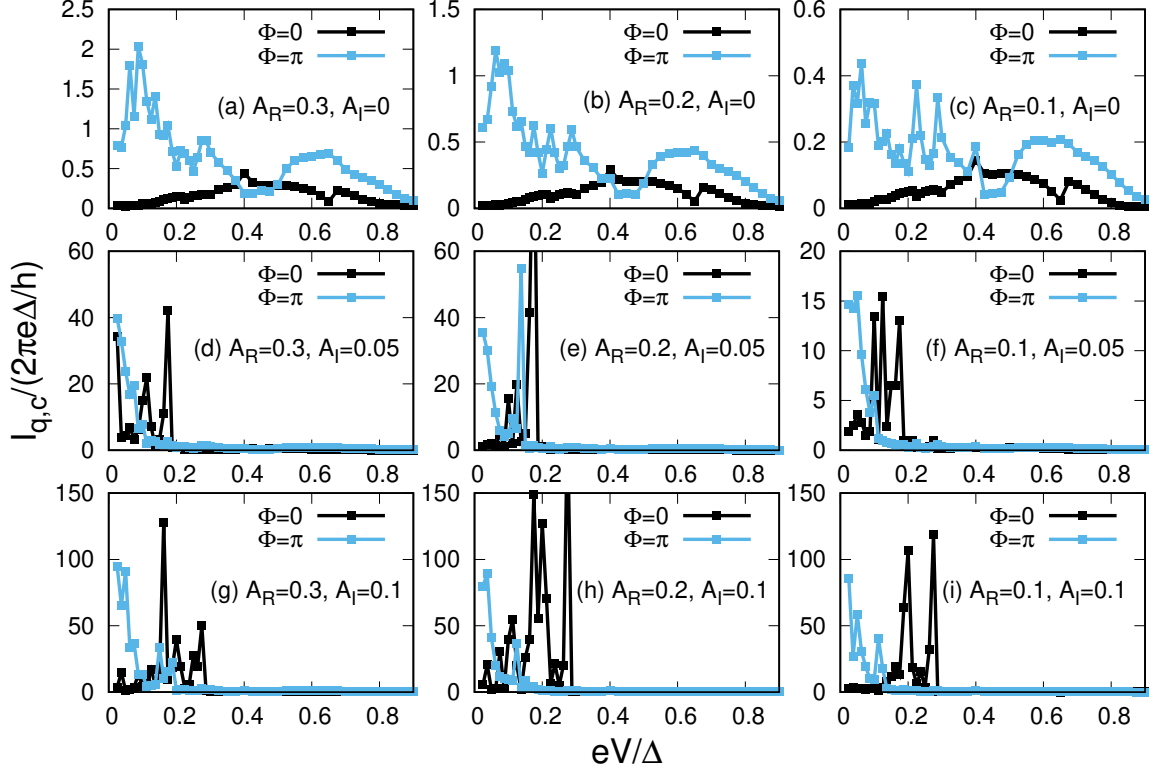


FIG. 7. The eV/Δ -dependence of the quartet critical current. Each panel of this figure shows $I_{q,c}(eV/\Delta, \Phi = 0)$ and $I_{q,c}(\Phi = \pi, eV/\Delta)$ as a function of the normalized bias voltage eV/Δ , for $A_I = 0$ and $A_R = 0.3/W$ (a), $A_R = 0.2/W$ (b) and $A_R = 0.1/W$ (c). Panels d, e and f correspond to $A_I = 0.05/W$ and $A_R = 0.3/W$ (d), $A_R = 0.2/W$ (e) and $A_R = 0.1/W$ (f) and panels g, h, i show $I_{q,c}(\Phi = 0, eV/\Delta)$ and $I_{q,c}(\Phi = \pi, eV/\Delta)$ for $A_I = 0.1/W$ and $A_R = 0.3/W$ (g), $A_R = 0.2/W$ (h) and $A_R = 0.1/W$ (i). We use $\Gamma/\Delta = 1$, $\Gamma'/\Delta = 0$, $B_R = B_I = 0$, and $\varepsilon_x = \varepsilon_y = 0$. The notation W is used for the band-width.

and 7g, 7h, 7i respectively. The numerical results in figure 7 are in agreement with the general mechanism of section III.

Figure 8 shows the normalized voltage- eV/Δ -dependence of the quartet critical current $I_{q,c}$, in semi-logarithmic scale, now with nonvanishingly small $\lambda = \Gamma'/\Gamma$, and with $A_I = 0.05/W$. Those sharp peaks in the quartet critical current are expected to change as the value of the normal metal Green's functions is varied in Eqs. (53)-(56). The quartet critical current plotted as a function of the bias voltage V is normal in log-scale. The corresponding peaks are expected to evolve as $k_F R_0$ is varied and thus, sample-to-sample fluctuations are expected to have log-normal distribution.

In addition, multiple cross-overs are obtained in figure 8 between $I_{q,c}(\Phi = \pi, eV/\Delta) - I_{q,c}(\Phi = 0, eV/\Delta) > 0$ (i.e. inversion) and $I_{q,c}(\Phi = \pi, eV/\Delta) - I_{q,c}(\Phi = 0, eV/\Delta) < 0$ (i.e. noninverted behavior) in a low-voltage window.

Figure 9 shows the sign of $I_{q,c}(\lambda, \Phi = \pi, eV/\Delta) - I_{q,c}(\lambda, \Phi = 0, eV/\Delta)$ as a function of the parameters $\lambda = \Gamma'/\Gamma$ (on the x-axis) and eV/Δ (on the y-axis). Inversion $I_{q,c}(\lambda, \Phi = \pi, eV/\Delta) - I_{q,c}(\lambda, \Phi = 0, eV/\Delta) > 0$ is obtained at low eV/Δ for $\lambda = 0$, see the previous section IV and Appendix B for a discussion of the inversion in the $eV/\Delta = 0^+$ limit. In figure 9, increasing the coupling Γ' between D_x and $(S_b, S_{c,2})$ or

between D_y and $(S_a, S_{c,1})$ [in addition to Γ between D_x and $(S_a, S_{c,1})$ or between D_y and $(S_b, S_{c,2})$], makes the double 0D quantum dot behave closer to a pair of single quantum dots. This favors the “noninverted behavior” typical of single quantum dots, as opposed to the “inverted behavior” appearing at $\lambda = \Gamma'/\Gamma = 0$ in a double 0D quantum dot, see Appendix B.

The values $\lambda = \Gamma'/\Gamma$ such that $0.2 \lesssim \lambda \lesssim 0.6$ in figure 9 generically yield “inversion” at low bias-voltage V , followed by “absence of inversion” at higher V -values. Now, we show that “absence of inversion” can appear at low bias-voltage V if we include the on-site energies $\varepsilon_x = \varepsilon_y \equiv \varepsilon_0$ in the double quantum dot Hamiltonian given by Eqs. (4)-(5). Namely, the parameter $\lambda = \Gamma'/\Gamma$ is set to $\lambda = 1/2$ in figure 10. Moving away from $\varepsilon_0/\Delta = 0$ in figure 10 produces typical voltage-dependence of $I_{q,c}(\lambda, \Phi = \pi, eV/\Delta) - I_{q,c}(\lambda, \Phi = 0, eV/\Delta)$ with “noninverted behavior” at low $V < V_*$ and “inversion” at higher $V > V_*$, see for instance the moderately small values $-0.5 \lesssim \varepsilon_0/\Delta \lesssim 0.5$ in figure 10. With the considered parameters, the ratio eV_*/Δ is in the range $eV_*/\Delta \approx 0.1$. Thus, our model is compatible with the experimental data [61] shown in figure 1b.

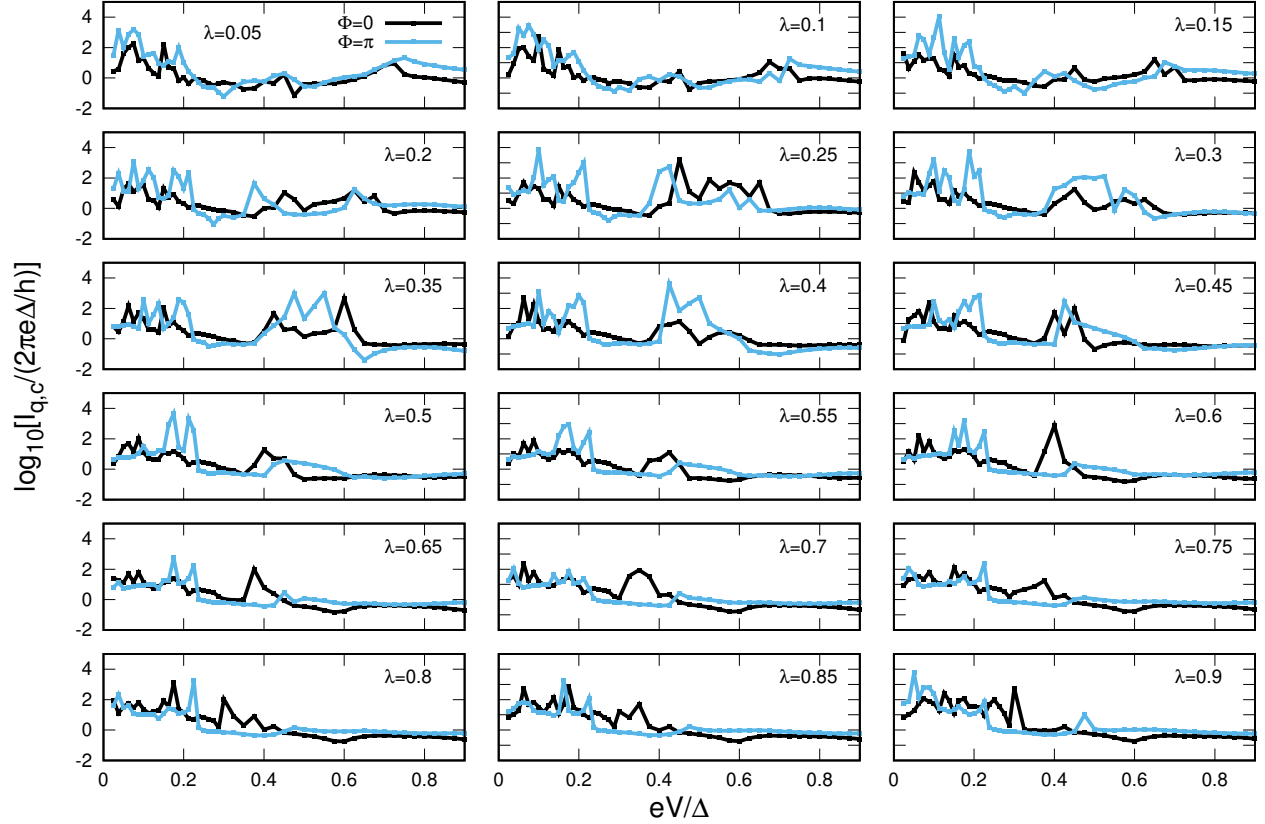


FIG. 8. The eV/Δ -dependence of the quartet critical current. The figure shows the reduced voltage- eV/Δ -dependence of the logarithm of the quartet critical currents $\log_{10}(I_{q,c}(\Phi = 0, eV/\Delta))$ and $\log_{10}(I_{q,c}(\Phi = \pi, eV/\Delta))$ at $\Phi = 0$ and $\Phi = \pi$ respectively. The panels show increasing values of $\lambda = \Gamma'/\Gamma$, where Γ is the “direct” coupling between D_x and S_a , $S_{c,1}$ and between D_y and S_b , $S_{c,2}$. The crossed coupling Γ' is in between D_x and S_b , $S_{c,2}$ and between D_y and S_a , $S_{c,1}$. We used $\Gamma/\Delta = 1$, $A_R = 0.3/W$, $A_I = 0.05/W$, and $B_R = B_I = 0$, where W is the band-width. The on-site energies $\varepsilon_x = \varepsilon_y = 0$ are vanishingly small.

VI. CONCLUSIONS

Now, we provide final remarks. The paper is summarized in subsection VI A, and perspectives are presented in subsection VI B.

A. Summary of the paper

Now, we summarize the paper.

We proposed models of ballistic multiterminal Josephson junctions made with superconducting leads evaporated on a 2D metal. The model consists of a multilevel quantum dot connected to superconducting and normal leads. We argued that the qualitative physics of the two-Cooper pair resonance can be captured with phenomenological double quantum dots connected to superconducting and normal leads. The coupling to the nonproximitized regions of the ballistic conductor produces relaxation, and a fraction of the quartet-phase sensitive

current is transmitted into the normal parts of the circuit.

We found resonances in calculations that account for both the time-periodic dynamics and small relaxation, if the multilevel or double quantum dot support levels at opposite energies. A related effect was previously found in the thermal noise of a superconducting weak link [90].

Noninverted-to-inverted cross-over numerically emerges as the bias voltage increases, where “inversion” means “larger quartet critical current at half flux-quantum $\Phi = \pi$ than in zero field at $\Phi = 0$ ”. The corresponding cross-over voltage V_* is small compared to the superconducting, typically $eV_* \approx \Delta/10$ with the parameters of our calculations, which is compatible with the recent Harvard group experiment [61].

B. Perspectives

A challenge for the theory is to model devices that are quite complex, with e.g. extended interfaces, four or more

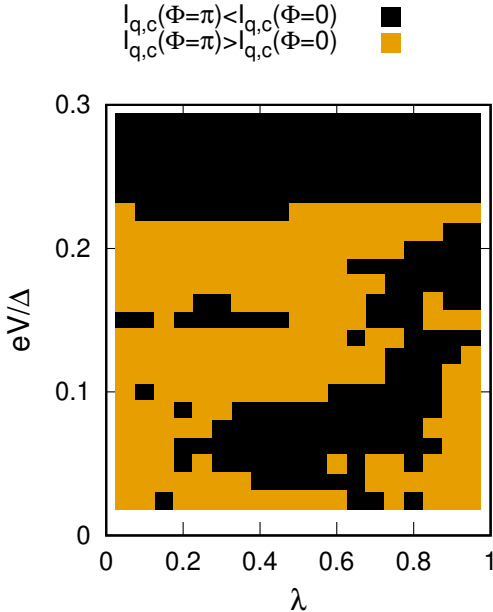


FIG. 9. *The sign of the inversion.* The figure shows the sign of $I_{q,c}(\lambda, \Phi = \pi, eV/\Delta) - I_{q,c}(\lambda, \Phi = 0, eV/\Delta)$, where $\lambda = \Gamma'/\Gamma$. Inversion corresponds to $I_{q,c}(\lambda, \Phi = \pi, eV/\Delta) - I_{q,c}(\lambda, \Phi = 0, eV/\Delta) > 0$. The parameter Γ is the “direct” coupling between D_x and $(S_a, S_{c,1})$ or between D_y and $(S_b, S_{c,2})$. The parameter Γ' is in between D_x and $(S_b, S_{c,2})$ or D_y and $(S_a, S_{c,1})$. We used $\Gamma/\Delta = 1$, $A_R = 0.3/W$, $A_I = 0.05/W$, and $B_R = B_I = 0$, where W is the band-width. The on-site energies $\varepsilon_x = \varepsilon_y = 0$ are vanishingly small.

superconducting leads, nonequilibrium voltage biasing conditions, loops connecting superconducting terminals, possibly with radio-frequency radiation. Direct diagonalizations of the Bogoliubov-de Gennes Hamiltonian would apparently lead to prohibitive computational expenses. In the field of mesoscopic superconductivity, Nazarov and co-workers (see Ref. 96 and references therein) proposed and developed finite element theory for the superconducting-normal metal circuits that describe the proximity effect, i.e. the interplay between Andreev reflection and multiple scattering on disorder. This dirty-limit circuit theory was proposed for multi-terminal Josephson junctions [68, 97]. The dirty limit implies short elastic mean free path, a condition that is not directly met in the ballistic metals that are currently used in some experiments on superconducting hybrid structures, such as carbon nanotubes [98], semiconducting nanowires [66] or graphene [84, 99, 100]. Specifically, tunneling spectroscopy of carbon nanotube Josephson junctions [98] revealed discrete ABS. Andreev molecules were realized with semiconducting nanowires [66]. Evidence for superconducting phase difference-sensitive continuum of ABS was obtained in superconductor-graphene-superconductor Josephson junctions [99, 100]. As it is mentioned above, microwave experiments on short superconductor-graphene-superconductor Josephson junctions were recently carried out, and modeled with single-level quantum dots [84].

Several issues related to averaging could be investigated in

the future:

First, it would be interesting to numerically average over a distribution of the nonlocal Green’s function for double 0D quantum dots. A related issue is to implement quantum dots having dimension that is large compared to the Fermi wavelength λ_F instead of the 0D quantum dots of the present paper. On the other hand, the regime of weak sample-to-sample fluctuations of the quartet critical current can be addressed with quasiclassics. For instance, discretized Usadel equations were used to calculate multiple Andreev reflections in two-terminal devices in the dirty limit [101] and three-terminal devices were addressed within assumptions about the interface transparencies, also with Usadel equations [42].

Second, the use of Nazarov’s circuit theory implies that the Green’s function is uniform within a node, which is also satisfied by ballistic chaotic cavities [102]. Thus Nazarov’s circuit theory is also appropriate to describe a ballistic device if the coupling to the terminals is made through interfaces with small cross-sections, to ensure that the metal behaves like a chaotic cavity.

Third, an interesting perspective is to solve Eilenberger equations for the four-terminal device shown in figure 1.

Fourth, it would also be interesting to average over voltage fluctuations, the strength of which being controlled by the electromagnetic environment.

To conclude, perspectives are about the interplay between: (i) The “Floquet effects” that produce “non-selfaveraging-like” sharp resonance peaks in the voltage-dependence of the quartet signal for single-channel contacts, and (ii) The effect of averaging in space over extended contacts or in energy over the voltage fluctuations induced by the electromagnetic environment.

ACKNOWLEDGEMENTS

The author wishes to thank K. Huang, Y. Ronen and P. Kim for stimulating discussions about their experiment. The author wishes to thank R. Danneau for useful discussions and comments on the manuscript, and F. Levy-Bertrand and her colleagues H. Cercellier, K. Hasselbach, M.A. Measson for useful remarks during an informal seminar on this topic. The author thanks the Infrastructure de Calcul Intensif et de Données (GRICAD) for use of the resources of the Mésocentre de Calcul Intensif de l’Université Grenoble-Alpes (CIMENT). The author acknowledges support from the French National Research Agency (ANR) in the framework of the Graphmon project (ANR-19-CE47-0007).

Appendix A: Evolution in the weak-coupling limit of a quartet created at time $t = 0$

In this Appendix, we consider the “phenomenological model of double 0D quantum dots with normal lead in series”, see subsection II B 3, and evaluate the spectrum and the time-evolution of a quartet created at time $t = 0$.

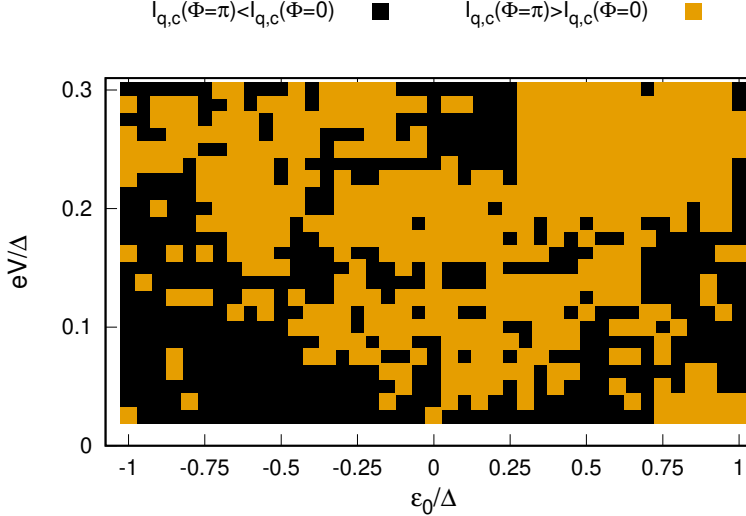


FIG. 10. *The sign of the inversion.* The figure is similar to the previous figure 9, but now the sign of $I_{q,c}(\epsilon_0/\Delta, \Phi = \pi, eV/\Delta) - I_{q,c}(\epsilon_0, \Phi = 0, eV/\Delta)$ is shown in the $(\epsilon_0/\Delta, eV/\Delta)$ plane. We used $\Gamma/\Delta = 1$, $A_R = 0.3/W$, $A_I = 0.05/W$, $B_R = B_I = 0$ (where W is the band-width) and $\lambda = \Gamma'/\Gamma = 1/2$. The on-site energies are identical for both quantum dots: $\epsilon_x = \epsilon_y = \epsilon_0$.

Calculation of the spectrum: We start with the simple limit where the four superconducting leads are disconnected, i.e. $\Gamma = \Gamma' = 0$, and consider that the two quantum dots D_x and D_y are connected to the tight-binding sites N'_x and N'_y by the tunneling amplitudes $\Sigma_{N'_x, D_x}^{(4)} = \Sigma_{D_x, N'_x}^{(4)}$ and $\Sigma_{N'_y, D_y}^{(4)} = \Sigma_{D_y, N'_y}^{(4)}$. The tight-binding sites are self-connected by the Green's functions $g_{N'_x, N'_x}$ and $g_{N'_y, N'_y}$, and connected to each other by the nonlocal Green's functions $g_{N'_x, N'_y} = g_{N'_y, N'_x}$. We denote by $g_{D_x, D_x}^A = g_{D_y, D_y}^A = 1/(\omega - i\eta)$ the Green's functions of the “isolated” quantum dots D_x and D_y , see Eqs. (7)-(8) where $\epsilon_x = \epsilon_y = 0$ in Eqs. (4)-(5). In addition \tilde{g}_{D_x, D_x} , \tilde{g}_{D_y, D_y} are their counterparts for the connected double 0D quantum dot, and by \tilde{g}_{D_x, D_y} and \tilde{g}_{D_y, D_x} are the corresponding nonlocal Green's functions. The Dyson equations relate the gs to the \tilde{g} s according to

$$\begin{aligned} \tilde{g}_{D_x, D_x} &= g_{D_x, D_x} + g_{D_x, D_x} \Sigma_{D_x, N'_x}^{(4)} g_{N'_x, N'_x} \Sigma_{N'_x, D_x}^{(4)} \tilde{g}_{D_x, D_x} \quad (A1) \\ &\quad + g_{D_x, D_x} \Sigma_{D_x, N'_x}^{(4)} g_{N'_x, N'_y} \Sigma_{N'_y, D_y}^{(4)} \tilde{g}_{D_y, D_x} \end{aligned}$$

$$\begin{aligned} \tilde{g}_{D_y, D_x} &= g_{D_y, D_y} \Sigma_{D_y, N'_y}^{(4)} g_{N'_y, N'_x} \Sigma_{N'_x, D_x}^{(4)} \tilde{g}_{D_x, D_x} \quad (A2) \\ &\quad + g_{D_y, D_y} \Sigma_{D_y, N'_y}^{(4)} g_{N'_y, N'_y} \Sigma_{N'_y, D_y}^{(4)} \tilde{g}_{D_y, D_x}, \quad (A3) \end{aligned}$$

which leads to the secular equation

$$\begin{vmatrix} \omega - \Gamma_{D_x, N'_x, N'_x, D_x} & -\Gamma_{D_x, N'_x, N'_y, D_y} \\ -\Gamma_{D_y, N'_y, N'_x, D_x} & \omega - \Gamma_{D_y, N'_y, N'_y, D_y} \end{vmatrix} = 0, \quad (A4)$$

where $\Gamma_{D_x, N'_x, N'_x, D_x} = \Sigma_{D_x, N'_x}^{(4)} g_{N'_x, N'_x} \Sigma_{N'_x, D_x}^{(4)}$, $\Gamma_{D_y, N'_y, N'_y, D_y} = \Sigma_{D_y, N'_y}^{(4)} g_{N'_y, N'_y} \Sigma_{N'_y, D_y}^{(4)}$, $\Gamma_{D_x, N'_x, N'_y, D_y} = \Sigma_{D_x, N'_x}^{(4)} g_{N'_x, N'_y} \Sigma_{N'_y, D_y}^{(4)}$, $\Gamma_{D_y, N'_y, N'_x, D_x} = \Sigma_{D_y, N'_y}^{(4)} g_{N'_y, N'_x} \Sigma_{N'_x, D_x}^{(4)}$. Assuming symmetric contacts yields $\Gamma_{D_x, N'_x, N'_x, D_x} = \Gamma_{D_y, N'_y, N'_y, D_y} \equiv \Gamma_{loc}$ and $\Gamma_{D_x, N'_x, N'_y, D_y} = \Gamma_{D_y, N'_y, N'_x, D_x} \equiv \Gamma_{nonloc}$. The energy levels are

given by

$$\omega_{(\pm)} = \Gamma_{loc} \pm \Gamma_{nonloc} \quad (A5)$$

$$= \left(\Sigma^{(4)} \right)^2 [B_R \pm A_R] + i \left(\Sigma^{(4)} \right)^2 [B_I \pm A_I], \quad (A6)$$

where A_R , A_I , B_R and B_I are given by Eqs. (53)-(56).

Evolution of a quartet created at time $t = 0$: Assuming tunnel coupling between the superconductors and the double quantum dot, a quartet created at time $t = 0$ in the state

$$|Q(0)\rangle = c_{\omega_{(+)}, \uparrow}^+(0) c_{\omega_{(+)}, \downarrow}^+(0) c_{\omega_{(-)}, \uparrow}^+(0) c_{\omega_{(-)}, \downarrow}^+(0) \quad (A7)$$

freely evolves according to

$$|Q(\tau)\rangle = \exp(-i\mathcal{H}_{dot}\tau) |Q(0)\rangle \quad (A8)$$

$$= \exp[-2i(\text{Re}(\omega_{(+)}) + \text{Re}(\omega_{(-)}))\tau] \times \quad (A9)$$

$$\exp[2(\text{Im}(\omega_{(+)}) + \text{Im}(\omega_{(-)}))\tau] |Q(0)\rangle.$$

Now, we assume $B_R = B_I = 0$, as in section V. Then, Eqs. (A5)-(A6) yield energy levels $\omega_{(\pm)} = \pm \Sigma^{(4)} (A_R + iA_I)$ having opposite real and imaginary parts, as it is expected for non-Hermitian Hamiltonians. Eqs. (A8)-(A9) become static:

$$|Q(\tau)\rangle = |Q(0)\rangle. \quad (A10)$$

Conclusions: Eq. (A10) implies that, within the weak-coupling limit, a quartet created at time $t = 0$ neither dephases nor relaxes. This stability can be seen as being compatible with enhanced quartet current in double 0D quantum dot configurations. Conversely, the single 0D quantum dots of our previous paper II [52] would produce $|Q(0)\rangle = 0$, automatically leading to $|Q(\tau)\rangle = 0$.

Appendix B: $V = 0^+$ adiabatic limit

In this Appendix, we examine the $V = 0^+$ adiabatic limit of four-terminal Josephson junctions containing a single or two quantum dots (see subsections B 1 and B 2 below).

1. Single quantum dot

We start with single 0D quantum dots in the $V = 0^+$ adiabatic limit, summarizing a fraction of the Supplemental Material of our previous paper II [52].

The Dyson equations take the following form for the considered 0D quantum dot connected to p_0 superconducting leads by the tunnel amplitudes $\hat{\Sigma}_{D_x, S_{np}}^{(5)} = \hat{\Sigma}_{S_{np}, D_x}^{(5)}$, with $n_p = 1, \dots, p_0$:

$$\hat{G}_{D_x, D_x} = \hat{g}_{D_x, D_x} + \hat{g}_{D_x, D_x} \sum_{n_p=1}^{p_0} \hat{\Sigma}_{D_x, S_{np}}^{(5)} \hat{g}_{S_{np}, S_{np}} \hat{\Sigma}_{S_{np}, D_x}^{(5)} \hat{G}_{D_x, D_x}. \quad (\text{B1})$$

In the infinite-gap limit, Eq. (B1) can be expressed with the infinite-gap Hamiltonian $\hat{\mathcal{H}}_{eff, singledot}^{(\infty)}$:

$$\hat{G}_{D_x, D_x}^A = \left(\omega - i\eta - \hat{\mathcal{H}}_{eff, singledot}^{(\infty)} \right)^{-1}, \quad (\text{B2})$$

where

$$\hat{\mathcal{H}}_{eff, singledot}^{(\infty)} = \sum_{n_p=1}^{p_0} \hat{\Sigma}_{D_x, S_{np}}^{(5)} \hat{g}_{S_{np}, S_{np}} \hat{\Sigma}_{S_{np}, D_x}^{(5)}. \quad (\text{B3})$$

Specifically, we obtain the following with $p_0 = 4$ supercon-

ducting leads:

$$\hat{\mathcal{H}}_{eff, singledot}^{(\infty)} = \begin{pmatrix} 0 & \gamma_{D_x, D_x} \\ (\gamma_{D_x, D_x})^* & 0 \end{pmatrix}, \quad (\text{B4})$$

where

$$\begin{aligned} \gamma_{D_x, D_x} &= \Gamma_a \exp(i\varphi_a) + \Gamma_b \exp(i\varphi_b) \\ &+ \Gamma_{c,1} \exp(i\varphi_{c,1}) + \Gamma_{c,2} \exp(i\varphi_{c,2}), \end{aligned} \quad (\text{B5})$$

and $\Gamma_{n_p} = \left(\Sigma_{D_x, S_{np}}^{(5)} \right)^2 / W$ parameterizes the line-width broadening of the quantum dot level in the normal state.

The $(S_{c,1}, S_{c,2})$ superconducting leads can be gathered into the single $S_{c,eff}$ coupled by

$$\Gamma_{c,eff} = \Gamma_{c,1} \exp(i\varphi_{c,1}) + \Gamma_{c,2} \exp(i\varphi_{c,2}). \quad (\text{B6})$$

Using the identical $\Gamma_{c,1} = \Gamma_{c,2} \equiv \Gamma_c$ and the gauge given by Eqs. (2)-(3) yields

$$\Gamma_{c,eff} = \Gamma_c [1 + \exp(i\Phi)] \exp(i\varphi_{c,1}). \quad (\text{B7})$$

It was shown in the Supplemental Material of our previous paper II [52] that nonsymmetric coupling to the superconducting leads can produce inversion between $\Phi = 0$ and $\Phi = \pi$ in the infinite-gap limit. But Eq. (B7) implies $|\Gamma_{c,eff}| = 2\Gamma_c$ if $\Phi = 0$ and $\Gamma_{c,eff} = 0$ if $\Phi = \pi$ for symmetric couplings to the superconducting leads, *i.e.* the quartet current at $\Phi = \pi$ is vanishingly small, thus it is automatically smaller than at $\Phi = 0$.

2. Double 0D quantum dot

In this subsection, we provide simple argument for emergence of inversion in the double 0D quantum dot with normal lead in parallel in figure 3, in the limits $eV/\Delta = 0^+$ and $\Gamma' = 0$.

In the infinite-gap limit, the 4×4 Hamiltonian of a double 0D quantum dot with normal leads in parallel is given by

$$\hat{\mathcal{H}}_{eff, doubledot}^{(\infty)} = \begin{pmatrix} 0 & \gamma_{D_x, D_x} & \Sigma^{(0)} & 0 \\ (\gamma_{D_x, D_x})^* & 0 & 0 & -\Sigma^{(0)} \\ \Sigma^{(0)} & 0 & 0 & \gamma_{D_y, D_y} \\ 0 & -\Sigma^{(0)} & (\gamma_{D_y, D_y})^* & 0 \end{pmatrix}, \quad (\text{B8})$$

where we assumed $\Gamma' = 0$, and we use the notation

$$\gamma_{D_x, D_x} = \Gamma_a \exp(i\varphi_a) + \Gamma_{c,1} \exp(i\varphi_{c,1}) \quad (\text{B9})$$

$$\gamma_{D_y, D_y} = \Gamma_b \exp(i\varphi_b) + \Gamma_{c,2} \exp(i\varphi_{c,2}). \quad (\text{B10})$$

Squaring the infinite-gap Hamiltonian given by Eq. (B8) leads to

$$\left(\hat{\mathcal{H}}_{eff, double dot}^{(\infty)} \right)^2 = \begin{pmatrix} |\gamma_{D_x, D_x}|^2 + (\Sigma^{(0)})^2 & 0 & 0 & -\Sigma^{(0)} [\gamma_{D_x, D_x} - \gamma_{D_y, D_y}] \\ 0 & |\gamma_{D_x, D_x}|^2 + (\Sigma^{(0)})^2 & \Sigma^{(0)} [(\gamma_{D_x, D_x})^* - (\gamma_{D_y, D_y})^*] & 0 \\ 0 & \Sigma^{(0)} [\gamma_{D_x, D_x} - \gamma_{D_y, D_y}] & |\gamma_{D_y, D_y}|^2 + (\Sigma^{(0)})^2 & 0 \\ -\Sigma^{(0)} [(\gamma_{D_x, D_x})^* - (\gamma_{D_y, D_y})^*] & 0 & 0 & |\gamma_{D_y, D_y}|^2 + (\Sigma^{(0)})^2 \end{pmatrix}, \quad (B11)$$

which decouples into the following 2×2 blocks:

$$[\hat{\mathcal{H}}^2]_{2 \times 2}^{(0)} = \begin{pmatrix} |\gamma_{D_x, D_x}|^2 + (\Sigma^{(0)})^2 & -\Sigma^{(0)} [\gamma_{D_x, D_x} - \gamma_{D_y, D_y}] \\ -\Sigma^{(0)} [(\gamma_{D_x, D_x})^* - (\gamma_{D_y, D_y})^*] & |\gamma_{D_y, D_y}|^2 + (\Sigma^{(0)})^2 \end{pmatrix} \quad (B12)$$

and

$$[\hat{\mathcal{H}}^2]_{2 \times 2}^{(2)} = \begin{pmatrix} |\gamma_{D_x, D_x}|^2 + (\Sigma^{(0)})^2 & \Sigma^{(0)} [(\gamma_{D_x, D_x})^* - (\gamma_{D_y, D_y})^*] \\ \Sigma^{(0)} [\gamma_{D_x, D_x} - \gamma_{D_y, D_y}] & |\gamma_{D_y, D_y}|^2 + (\Sigma^{(0)})^2 \end{pmatrix}. \quad (B13)$$

Thus,

$$\begin{aligned} \gamma_{D_x, D_x} - \gamma_{D_y, D_y} &= \Gamma_a \exp(i\varphi_a) + \Gamma_{c,1} \exp(i\varphi_{c,1}) \quad (B14) \\ &\quad - \Gamma_b \exp(i\varphi_b) - \Gamma_{c,2} \exp(i\varphi_{c,2}) \end{aligned}$$

and the coupling to the effective $S_{c,eff}$ is now given by the difference

$$\Gamma_{c,eff} = \Gamma_{c,1} \exp(i\varphi_{c,1}) - \Gamma_{c,2} \exp(i\varphi_{c,2}) \quad (B15)$$

instead of the previous Eq. (B6) for a single 0D quantum dot. Eq. (B15) goes to

$$\Gamma_{c,eff}(\Phi) = \Gamma [1 - \exp(i\Phi)] \exp(i\varphi_{c,1}) \quad (B16)$$

in the considered limit $\Gamma_{c,1} = \Gamma_{c,2} \equiv \Gamma$ of symmetric couplings. Thus, the interference $|\Gamma_{c,eff}|(\Phi = 0) = 0$ and $|\Gamma_{c,eff}|(\Phi = \pi) = 2\Gamma$ yields inversion between $\Phi = 0$ and $\Phi = \pi$ with symmetric coupling to the superconducting leads. This contrasts with absence of inversion for single 0D quantum dots, see section B 1 in this Appendix.

[1] J. Bardeen, L. N. Cooper, and J. R. Schrieffer, *Theory of Superconductivity*, Phys. Rev. **108**, 1175 (1957).

[2] N. K. Allsopp, V. C. Hui, C. J. Lambert, and S. J. Robinson, *Theory of the sign of multi-probe conductances for normal and superconducting materials*, J. Phys.: Condens. Matter **6**, 10475 (1994).

[3] J. M. Byers and M. E. Flatté, *Probing Spatial Correlations with Nanoscale Two-Contact Tunneling*, Phys. Rev. Lett. **74**, 306 (1995).

[4] J. Torrès and T. Martin, *Positive and negative Hanbury-Brown and Twiss correlations in normal metal-superconducting devices*, Eur. Phys. J. B **12**, 319 (1999).

[5] G. Deutscher and D. Feinberg, *Coupling superconducting-ferromagnetic point contacts by Andreev reflections*, Appl. Phys. Lett. **76**, 487 (2000).

[6] M. S. Choi, C. Bruder, and D. Loss, *Spin-dependent Josephson current through double quantum dots and measurement of entangled electron states*, Phys. Rev. B **62**, 13569 (2000).

[7] G. Falci, D. Feinberg, and F. W. J. Hekking, *Correlated tunneling into a superconductor in a multiprobe hybrid structure*, Europhys. Lett. **54**, 255 (2001).

[8] P. Recher, E. V. Sukhorukov, and D. Loss, *Andreev tunneling, Coulomb blockade, and resonant transport of nonlocal spin-entangled electrons*, Phys. Rev. B **63**, 165314 (2001).

[9] G. B. Lesovik, T. Martin, and G. Blatter, *Electronic entanglement in the vicinity of a superconductor*, Eur. Phys. J. B **24**, 287 (2001).

[10] R. Mélin and D. Feinberg, *Transport theory of multiterminal hybrid structures*, Eur. Phys. J. B **26**, 101 (2002).

[11] N. M. Chtchelkatchev, G. Blatter, G. B. Lesovik, and T. Martin, *Bell inequalities and entanglement in solid-state devices*, Phys. Rev. B **66**, 161320 (2002).

[12] R. Mélin and D. Feinberg, *Sign of the crossed conductances at a ferromagnet/superconductor/ferromagnet double interface*, Phys. Rev. B **70**, 174509 (2004).

[13] A. V. Lebedev, G. B. Lesovik, and G. Blatter, *Generating spin-entangled electron pairs in normal conductors using voltage pulses*, Phys. Rev. B **72**, 245314 (2005).

[14] K. V. Bayandin, G. B. Lesovik, and T. Martin, *Energy entanglement in normal metal-superconducting forks* Phys. Rev. B

74, 085326 (2006).

[15] A. L. Yeyati, F. S. Bergeret, A. Martín-Rodero, and T. M. Klapwijk, *Entangled Andreev pairs and collective excitations in nanoscale superconductors*, *Nature Phys.* **3**, 455 (2007).

[16] D. Beckmann, H. B. Weber, and H. v. Löhneysen, *Evidence for crossed Andreev reflection in Superconductor-Ferromagnet hybrid structures*, *Phys. Rev. Lett.* **93**, 197003 (2004).

[17] S. Russo, M. Kroug, T. M. Klapwijk, and A. F. Morpurgo, *Experimental observation of bias-dependent nonlocal Andreev reflection*, *Phys. Rev. Lett.* **95**, 027002 (2005).

[18] P. Cadden-Zimansky and V. Chandrasekhar, *Nonlocal correlations in normal-metal superconducting systems*, *Phys. Rev. Lett.* **97**, 237003 (2006).

[19] D. Beckmann, H. B. Weber, and H. v. Löhneysen, *Negative four-terminal resistance as a probe of crossed Andreev reflection*, *Appl. Phys. A* **89**, 603 (2007).

[20] P. Cadden-Zimansky, Z. Jiang, and V. Chandrasekhar, *Charge imbalance, crossed Andreev reflection and elastic co-tunnelling in ferromagnet/superconductor/normal-metal structures*, *New J. Phys.* **9**, 116 (2007).

[21] L. Hofstetter, S. Csonka, J. Nygard, and C. Schönenberger, *Cooper pair splitter realized in a two-quantum-dot Y-junction*, *Nature (London)* **461**, 960 (2009).

[22] L. G. Herrmann, F. Portier, P. Roche, A. Levy Yeyati, T. Kontos, and C. Strunk, *Carbon nanotubes as Cooper pair beam splitters*, *Phys. Rev. Lett.* **104**, 026801 (2010).

[23] J. Wei and V. Chandrasekhar, *Positive noise cross-correlation in hybrid superconducting and normal-metal three-terminal devices*, *Nat. Phys.* **6**, 494 (2010).

[24] A. Das, Y. Ronen, M. Heiblum, D. Mahalu, A. V. Kretinin, and H. Shtrikman, *High-efficiency Cooper pair splitting demonstrated by two-particle conductance resonance and positive noise cross-correlation*, *Nat. Commun.* **3**, 1165 (2012).

[25] J. Schindele, A. Baumgartner, and C. Schönenberger, *Near-Unity Cooper Pair Splitting Efficiency*, *Phys. Rev. Lett.* **109**, 157002 (2012).

[26] J. Schindele, A. Baumgartner, R. Maurand, M. Weiss, and C. Schönenberger, *Nonlocal spectroscopy of Andreev bound states*, *Phys. Rev. B* **89**, 045422 (2014).

[27] Z. B. Tan, D. Cox, T. Nieminen, P. Lähteenmäki, D. Golubev, G. B. Lesovik, and P. J. Hakonen, *Cooper Pair Splitting by Means of Graphene Quantum Dots*, *Phys. Rev. Lett.* **114**, 096602 (2015).

[28] I. V. Borzenets, Y. Shimazaki, G. F. Jones, M. F. Craciun, S. Russo, M. Yamamoto, and S. Tarucha, *High Efficiency CVD Graphene-lead (Pb) Cooper Pair Splitter*, *Sci. Rep.* **6**, 23051 (2016).

[29] P. Pandey, R. Danneau, and D. Beckmann, *Ballistic Graphene Cooper Pair Splitter*, *Phys. Rev. Lett.* **126**, 147701 (2021).

[30] M. P. Anantram and S. Datta, *Current fluctuations in mesoscopic systems with Andreev scattering*, *Phys. Rev. B* **53**, 16390 (1996).

[31] P. Samuelsson and M. Büttiker, *Chaotic dot-superconductor analog of the Hanbury Brown-Twiss effect*, *Phys. Rev. Lett.* **89**, 046601 (2002).

[32] P. Samuelsson and M. Büttiker, *Semiclassical theory of current correlations in chaotic dot-superconductor systems*, *Phys. Rev. B* **66**, 201306 (R) (2002).

[33] J. Börlin, W. Belzig, and C. Bruder, *Full counting statistics of a superconducting beam splitter*, *Phys. Rev. Lett.* **88**, 197001 (2002).

[34] P. Samuelsson, E.V. Sukhorukov, and M. Büttiker, *Orbital entanglement and violation of Bell inequalities in mesoscopic conductors*, *Phys. Rev. Lett.* **91**, 157002 (2003).

[35] L. Faoro, F. Taddei, and R. Fazio, *Clauser-Horne inequality for electron-counting statistics in multiterminal mesoscopic conductors*, *Phys. Rev. B* **69**, 125326 (2004).

[36] G. Bignon, M. Houzet, F. Pistolesi, and F.W.J. Hekking, *Current-current correlations in hybrid superconducting and normal metal multiterminal structures*, *Europhys. Lett.* **67**, 110 (2004).

[37] R. Mélin, C. Benjamin, and T. Martin, *Positive cross correlations of noise in superconducting hybrid structures: Roles of interfaces and interactions*, *Phys. Rev. B* **77**, 094512 (2008).

[38] A. Freyn, M. Flöser and R. Mélin, *Positive current cross-correlations in a highly transparent normal-superconducting beam splitter due to synchronized Andreev and inverse Andreev reflections*, *Phys. Rev. B* **82**, 014510 (2010).

[39] D.S. Golubev and A.D. Zaikin, *Shot noise and Coulomb effects on nonlocal electron transport in normal-metal/superconductor/normal-metal heterostructures*, *Phys. Rev. B* **82**, 134508 (2010).

[40] M. Flöser, D. Feinberg and R. Mélin, *Absence of split pairs in cross correlations of a highly transparent normal metal-superconductor-normal metal electron-beam splitter*, *Phys. Rev. B* **88**, 094517 (2013).

[41] G. Michalek, B. R. Bulka, T. Domański, and K. I. Wysokiński, *Statistical correlations of currents flowing through a proximitized quantum dot*, *Phys. Rev. B* **101**, 235402 (2020).

[42] J. C. Cuevas and H. Pothier, *Voltage-induced Shapiro steps in a superconducting multiterminal structure*, *Phys. Rev. B* **75**, 174513 (2007).

[43] A. Freyn, B. Douçot, D. Feinberg, and R. Mélin, *Production of non-local quartets and phase-sensitive entanglement in a superconducting beam splitter*, *Phys. Rev. Lett.* **106**, 257005 (2011).

[44] T. Jonckheere, J. Rech, T. Martin, B. Douçot, D. Feinberg, and R. Mélin, *Multipair DC Josephson resonances in a biased all-superconducting bijunction*, *Phys. Rev. B* **87**, 214501 (2013).

[45] R. Mélin, D. Feinberg, and B. Douçot, *Partially resummed perturbation theory for multiple Andreev reflections in a short three-terminal Josephson junction*, *Eur. Phys. J. B* **89**, 67 (2016).

[46] R. Mélin, M. Sotto, D. Feinberg, J.-G. Caputo and B. Douçot, *Gate-tunable zero-frequency current cross-correlations of the quartet mode in a voltage-biased three-terminal Josephson junction*, *Phys. Rev. B* **93**, 115436 (2016).

[47] R. Mélin, J.-G. Caputo, K. Yang and B. Douçot, *Simple Floquet-Wannier-Stark-Andreev viewpoint and emergence of low-energy scales in a voltage-biased three-terminal Josephson junction*, *Phys. Rev. B* **95**, 085415 (2017).

[48] R. Mélin, R. Danneau, K. Yang, J.-G. Caputo, and B. Douçot, *Engineering the Floquet spectrum of superconducting multiterminal quantum dots*, *Phys. Rev. B* **100**, 035450 (2019).

[49] J.D. Pillet, V. Benzoni, J. Griesmar, J.-L. Smirr, and Ç.Ö. Girit, *Nonlocal Josephson Effect in Andreev Molecules* *Nano Lett.* **19**, 7138 (2019).

[50] V. Kornich, H.S. Barakov, and Yu.V. Nazarov, *Fine energy splitting of overlapping Andreev bound states in multiterminal superconducting nanostructures*, *Phys. Rev. Research* **1**, 033004 (2019).

[51] R. Mélin and B. Douçot, *Inversion in a four terminal superconducting device on the quartet line. I. Two-dimensional metal and the quartet beam splitter*, *Phys. Rev. B* **102**, 245435 (2020).

[52] R. Mélin and B. Douçot, *Inversion in a four terminal superconducting device on the quartet line. II. Quantum dot and Floquet theory*, *Phys. Rev. B* **102**, 245436 (2020).

[53] J.-D. Pillet, V. Benzoni, J. Griesmar, J.-L. Smirr, and Ç. Ö. Girit, *Scattering description of Andreev molecules*, SciPost Phys. Core **2**, 009 (2020).

[54] V. Kornich, H. S. Barakov and Yu. V. Nazarov, *Overlapping Andreev states in semiconducting nanowires: competition of 1D and 3D propagation*, Phys. Rev. B **101**, 195430 (2020).

[55] R. Mélin, *Ultralong-distance quantum correlations in three-terminal Josephson junctions*, Phys. Rev. B **104**, 075402 (2021).

[56] A. Melo, V. Fatemi and A.R. Akhmerov, *Multiplet supercurrent in Josephson tunneling circuits*, arXiv:2104.11239 (2021).

[57] A.H. Pfeffer, J.E. Duvauchelle, H. Courtois, R. Mélin, D. Feinberg, and F. Lefloch, *Subgap structure in the conductance of a three-terminal Josephson junction*, Phys. Rev. B **90**, 075401 (2014).

[58] E. Strambini, S. D'Ambrosio, F. Vischi, F.S. Bergeret, Yu.V. Nazarov, and F. Giazotto, *The ω -SQUIPT as a tool to phase-engineer Josephson topological materials*, Nat. Nanotechnol. **11**, 1055 (2016).

[59] Y. Cohen, Y. Ronen, J.H. Kang, M. Heiblum, D. Feinberg, R. Mélin, and H. Strikman, *Non-local supercurrent of quartets in a three-terminal Josephson junction*, Proc. Natl. Acad. Sci. U. S. A. **115**, 6991 (2018).

[60] A.W. Draelos, M.-T. Wei, A. Seredinski, H. Li, Y. Mehta, K. Watanabe, T. Taniguchi, I.V. Borzenets, F. Amet, and G. Finkelstein, *Supercurrent flow in multiterminal graphene Josephson junctions*, Nano Lett. **19**, 1039 (2019).

[61] K.F. Huang, Y. Ronen, R. Mélin, D. Feinberg, K. Watanabe, T. Taniguchi, and P. Kim, *Quartet supercurrent in a multi-terminal Graphene-based Josephson Junction*, arXiv:2008.03419 (2020).

[62] N. Pankratova, H. Lee, R. Kuzmin, K. Wickramasinghe, J. W. Mayer, J. Yuan, M. Vavilov, J. Shabani and V. Manucharyan, *The multi-terminal Josephson effect*, Phys. Rev. X **10**, 031051 (2020).

[63] G.V. Graziano, J.S. Lee, M. Pendharkar, C. Palmstrom and V.S. Pribiag, *Transport Studies in a Gate-Tunable Three-Terminal Josephson Junction*, arXiv:1905.11730v2 (2020).

[64] E.G. Arnault, T. Larson, A. Seredinski, L. Zhao, H. Li, K. Watanabe, T. Taniguchi, I. Borzenets, F. Amet and G. Finkelstein, *The multiterminal inverse AC Josephson effect*, arXiv:2012.15253v1 (2020).

[65] S.A. Khan, L. Stampfer, T. Mutas, J.-H. Kang, P. Krogstrup and T.S. Jespersen, *Multiterminal Quantized Conductance in InSb Nanocrosses*, arXiv:2101.02529 (2021).

[66] O. Kürtössy, Z. Scherübl, G. Fülop, I. E. Lukács, T. Kanne, J. Nygård, P. Makk and S. Csonka, *Andreev molecule in parallel InAs nanowires*, arXiv:2103.14083 (2021).

[67] B. van Heck, S. Mi, and A.R. Akhmerov, *Single fermion manipulation via superconducting phase differences in multiterminal Josephson junctions*, Phys. Rev. B **90**, 155450 (2014).

[68] C. Padurariu, T. Jonckheere, J. Rech, R. Mélin, D. Feinberg, T. Martin, and Yu.V. Nazarov, *Closing the proximity gap in a metallic Josephson junction between three superconductors*, Phys. Rev. B **92**, 205409 (2015).

[69] R.-P. Riwar, M. Houzet, J.S. Meyer, and Y.V. Nazarov, *Multiterminal Josephson junctions as topological materials*, Nat. Commun. **7**, 11167 (2016).

[70] E. Eriksson, R.-P. Riwar, M. Houzet, J. S. Meyer, and Y. V. Nazarov, *Topological transconductance quantization in a four-terminal Josephson junction*, Phys. Rev. B **95**, 075417 (2017).

[71] O. Deb, K. Sengupta and D. Sen, *Josephson junctions of multiple superconducting wires*, Phys. Rev. B **97**, 174518 (2018).

[72] V. Fatem, A.R. Akhmerov and L. Bretheau, *Weyl Josephson circuits*, arXiv:2008.13758v1 (2020).

[73] L. Peyruchat, J. Griesmar, J.-D. Pillet and Ç.Ö. Girit, *Transconductance quantization in a topological Josephson tunnel junction circuit*, arXiv:2009.03291v1 (2020).

[74] H. Weisbrich, R.L. Klees, G. Rastelli and W. Belzig, *Second Chern Number and Non-Abelian Berry Phase in Topological Superconducting Systems*, PRX Quantum **2**, 010310 (2021).

[75] Y. Chen and Y.V. Nazarov, *Weyl point immersed in a continuous spectrum: an example from superconducting nanostructures*, Phys. Rev. B **104**, 104506 (2021).

[76] Y. Chen and Y.V. Nazarov, *Spin-Weyl quantum unit: theoretical proposal*, Phys. Rev. B **103**, 045410 (2021).

[77] E.V. Repin and Y.V. Nazarov, *Weyl points in the multi-terminal Hybrid Superconductor-Semiconductor Nanowire devices*, arXiv:2010.11494v1 (2020).

[78] B. Douçot, R. Danneau, K. Yang, J.-G. Caputo and R. Mélin, *Berry phase in superconducting multiterminal quantum dots*, Phys. Rev. B **101**, 035411 (2020).

[79] B. Venitucci, D. Feinberg, R. Mélin, B. Douçot, *Nonadiabatic Josephson current pumping by microwave irradiation*, Phys. Rev. B **97**, 195423 (2018).

[80] L.P. Gavensky, G. Usaj, D. Feinberg and C.A. Balseiro, *Berry curvature tomography and realization of topological Haldane model in driven three-terminal Josephson junctions*, Phys. Rev. B **97**, 220505 (2018).

[81] R. L. Klees, G. Rastelli, J. C. Cuevas, and W. Belzig, *Microwave Spectroscopy Reveals the Quantum Geometric Tensor of Topological Josephson Matter*, Phys. Rev. Lett. **124**, 197002 (2020).

[82] H.-Y. Xie, M.G. Vavilov and A. Levchenko, *Topological Andreev bands in three-terminal Josephson junctions*, Phys. Rev. B **96**, 161406 (2017).

[83] H.-Y. Xie, M.G. Vavilov and A. Levchenko, *Weyl nodes in Andreev spectra of multiterminal Josephson junctions: Chern numbers, conductances and supercurrents*, Phys. Rev. B **97**, 035443 (2018).

[84] S. Park, W. Lee, S. Jang, Y.-B. Choi, J. Park, W. Jung, K. Watanabe, T. Taniguchi, G. Y. Cho and G.-H. Lee, *Steady Floquet-Andreev States Probed by Tunneling Spectroscopy*, arXiv:2105.00592.

[85] S. B. Kaplan, C. C. Chi, D. N. Langenberg, J. J. Chang, S. Jafarey, and D. J. Scalapino, *Quasiparticle and phonon lifetimes in superconductors*, Phys. Rev. B **14**, 4854 (1976).

[86] R. C. Dynes, V. Narayanamurti, and J. P. Garno, *Direct measurement of quasiparticle-lifetime broadening in a strong-coupled superconductor*, Phys. Rev. Lett. **41**, 1509 (1978).

[87] J.P. Pekola, V. F. Maisi, S. Kafanov, N. Chekurov, A. Kemppinen, Yu. A. Pashkin, O.-P. Saira, M. Möttönen, and J. S. Tsai, *Environment-assisted tunneling as an origin of the Dynes density of states*, Phys. Rev. Lett. **105**, 026803 (2010).

[88] O.-P. Saira, A. Kemppinen, V. F. Maisi, and J. P. Pekola, *Vanishing quasiparticle density in a hybrid Al/Cu/Al single-electron transistor*, Phys. Rev. B **85**, 012504 (2012).

[89] F. S. Bergeret, P. Virtanen, A. Ozacta, T. T. Heikkilä, and J. C. Cuevas Phys. Rev. B **84**, 054504 (2011).

[90] A. Martín-Rodero, A. Levy Yeyati, F.J. García-Vidal, *Thermal noise in superconducting quantum point contacts*, Phys. Rev. B **53**, R8891 (1996).

[91] A. Zazunov, V. S. Shumeiko, E. N. Bratus', J. Lantz, and G. Wendin, *Andreev Level Qubit*, Phys. Rev. Lett. **90**, 087003 (2003).

[92] T. Meng, S. Florens and P. Simon, *Self-consistent description*

of Andreev bound states in Josephson quantum dot devices, Phys. Rev. B **79**, 224521 (2009).

[93] D. Averin and H.T. Imam, *Supercurrent noise in quantum point contacts*, Phys. Rev. Lett. **76**, 3814 (1996).

[94] J. C. Cuevas, A. Martín-Rodero, and A. Levy Yeyati, *Hamiltonian approach to the transport properties of superconducting quantum point contacts*, Phys. Rev. B **54**, 7366 (1996).

[95] C. Caroli, R. Combescot, P. Nozières and D. Saint-James, *Direct calculation of the tunneling current*, Jour. Phys. C: Solid State Phys. **4**, 916 (1971).

[96] Yu.V. Nazarov and Y.M. Blanter, *Quantum transport*, Cambridge University Press (2012).

[97] C. Padurariu, T. Jonckheere, J. Rech, T. Martin, and D. Feinberg, *Tunable pseudogaps due to nonlocal coherent transport in voltage-biased three-terminal Josephson junctions*, Phys. Rev. B **95**, 205437 (2017).

[98] J.-D. Pillet, C. Quay, P. Morfin, C. Bena, A. Levy Yeyati, and P. Joyez, *Revealing the electronic structure of a carbon nanotube carrying a supercurrent*, Nature Physics **6**, 965 (2010).

[99] L. Bretheau, J. I-J. Wang, R. Pisoni, K. Watanabe, T. Taniguchi, P. Jarillo-Herrero, *Tunnelling Spectroscopy of Andreev States in Graphene*, Nature Physics **13**, 756 (2017).

[100] J. I-J. Wang, L. Bretheau, D. Rodan-Legrain, R. Pisoni, K. Watanabe, T. Taniguchi, P. Jarillo-Herrero, *Tunneling spectroscopy of graphene nanodevices coupled to large-gap superconductors*, Phys. Rev. B **98**, 121411(R) (2018).

[101] J. C. Cuevas, J. Hammer, J. Kopu, J. K. Viljas, and M. Eschrig, *Proximity effect and multiple Andreev reflections in diffusive superconductor–normal-metal–superconductor junctions*, Phys. Rev. B **73**, 184505 (2006).

[102] M. Vanević and W. Belzig, *Full counting statistics of Andreev scattering in an asymmetric chaotic cavity*, Phys. Rev. B **72**, 134522 (2005).